From random point processes to hierarchical cavity master equations for stochastic dynamics of disordered systems in random graphs: Ising models and epidemics

D. Machado [*] and R. Mulet [†]

Group of Complex Systems and Statistical Physics. Department of Theoretical Physics, Physics Faculty, University of Havana, Cuba

(Received 10 July 2021; accepted 25 October 2021; published 15 November 2021)

We start from the theory of random point processes to derive n-point coupled master equations describing the continuous dynamics of discrete variables in random graphs. These equations constitute a hierarchical set of approximations that generalize and improve the cavity master equation (CME), a recently obtained closure for the usual master equation representing the dynamics. Our derivation clarifies some of the hypotheses and approximations that originally led to the CME, considered now as the first order of a more general technique. We tested the scheme in the dynamics of three models defined over diluted graphs: the Ising ferromagnet, the Viana-Bray spin-glass, and the susceptible-infectious-susceptible model for epidemics. In the first two, the equations perform similarly to the best-known approaches in literature. In the latter, they outperform the well-known pair quenched mean-field approximation.

DOI: 10.1103/PhysRevE.104.054303

I. INTRODUCTION

Emissions from a radioactive source, time series of electrical energy in a nerve fiber, the instants of arrival of customers in a queue, and the flips of a spin due to thermal activation are all examples of random processes that occur in such short intervals of time that can be classified as punctual. Sometimes the distinction between point processes and other stochastic processes is hard to define. For example, any stochastic process in continuous time in which the sample paths are step functions is associated with a point process, also any process with a discrete state space where a time of entry into a state occurs randomly.

The theory of random point processes (TRPP) [1,2] provides a formal and practical background to study and understand these and similar random collections of point occurrences. Usually, it is a matter of taste of the researchers or convenient for the research to attain, or not, the TRPP to approach a specific problem.

In this paper, we study the continuous dynamics of a system of discrete interacting variables. The model systems of interest can be viewed as a multivariate and multidimensional random point process. Alternatively, the dynamics of each variable can be considered as a random point process itself. We will show that starting from the TRPP it is possible to write hierarchical masterlike equations for any group of variables in the system.

An attempt in this direction was proposed a few years ago through the adaptation of dynamic message-passing equations from discrete-time to continuous-time dynamics. It landed first in the field of epidemics propagation [3,4] without a general formulation but with good results. Later, Ref. [5] proposed a closure for the master equation that exploited the TRPP. The core of this method is a differential equation for the cavity conditional probability densities: the cavity master equation (CME). This approach has proven to be very general as it has been applied to several models in graphs with finite connectivity like the Ising ferromagnet, the random field Ising model and the Viana-Bray spin-glass model [5], the ferromagnetic p-spin under Glauber dynamics [6], and, more recently, also the dynamics of a focused search algorithm to solve the random K-satisfiability (K-SAT) problem in the case with $K = 3$ [7]. In this paper, we generalize the CME derived in Ref. [5], providing master equations for the probability densities of any group of connected variables.

We concentrate on the continuous-time dynamics of discrete-spin variables. They can be described by a master equation for the probability density of the states of the system [8,9]. But to fully solve this master equation is a cumbersome task and results have been elusive, except for special cases. For example, the Sherrington-Kirkpatrick (SK) model in its nonsymmetric version has received preferential attention among the fully connected family [10,11], and the exact solution for parallel and asynchronous dynamics of the dilute fully asymmetric neural network model dates back to 1987 [12].

We provide here a general alternative solution that improves the approach presented in Ref. [5]. Although it is devised for single instances, it does not prevent its use to obtain global information. One can always numerically average the results of the integration of the single-instance equations. On the other hand, in Ref. [13] the CME equations were used as the starting point in the derivation of an average case description for the dynamics of the Ising ferromagnet, in this case defined on Erdos-Renyi random graphs.

To compute averaged quantities, one of the greatest advances in the field is the dynamical replica theory (DRT), introduced in Ref. [14]. This approach permits the

[*] dmachado@fisica.uh.cu
[†] mulet@fisica.uh.cu

derivation of average case equations for the probabilities of some macroscopic observables in fully connected [14,15] and diluted [16,17] graphs. In practice, DRT successfully reduces the dimensionality of the system, making the problem tractable. However, it also assumes that the microscopic probability distribution function is a constant within a subspace with a finite number of order parameters, something that has been put into question on specific models [18,19] and is not necessarily true for general nonequilibrium situations.

Another relevant approach to these problems is the scheme of analytical approximations introduced in Refs. [20,21] for the description of the dynamics of local search algorithms. In Ref. [22], this methodology is revisited and consolidated, also showing its equivalence to DRT under the assumption of replica symmetry. Due to its successful combination of accuracy and simplicity, we will come back to this scheme as a reference for evaluating our numerical results.

This paper contributes to the settlement of the dynamic cavity method as a general tool to study the continuous-time dynamics of discrete-spin models. A brief description of the theory of RPP is given in Sec. II. Section III presents our hierarchical system of corrections to the original equations derived in Ref. [5] and used in Refs. [6,7,13]. They are numerically tested in Sec. IV. We do not intend either to compare these directly with DRT, whose numerics we consider appreciably harder in this kind of graph, nor to give a better description of the dynamics of average quantities. Instead, we use the equivalent but simpler approximation schemes in Ref. [22] as a theoretical and numeric reference and as a proxy to the comparison with DRT.

Unlike the two approaches previously described, our method gives information about local probability distributions and can be straightforwardly used to study problems that are intrinsically out of equilibrium [7], i.e., where detailed balance is not conserved. As an example, Sec. IV C is devoted to the exploration of susceptible-infectious-susceptible (SIS) model for epidemics. Finally, Sec. V contains the conclusions of our paper.

II. RANDOM POINT PROCESSES

To facilitate the reading of Sec. III, we take a brief tour into the TRPP, which we will use to parametrize probability distributions of spin histories. After some basic definitions and for completeness, we will refer in Sec. II A to the simple case of an independent binary variable that randomly changes its state. There, we will use the random point processes formalism to derive a master equation for the variable's dynamics, and we will show how to extend this to the case of many interacting variables.

The core object of random point processes are spin trajectories or histories. For binary spin variables $\sigma = \pm 1$, a specific history that starts with $\sigma(t_0) = \sigma_0$ and ends with $\sigma(t) = \sigma$ is parametrized by the number of spin flips, the time in which they occur and the initial state of the system. Thus, we are in the presence of a random point process [1,2] where the probability measure may be denoted as

$$Q^t(X) = Q_s(t_0, t_1, ..., t_s, t|\sigma(t_0) = \sigma_0). \tag{1}$$

Equation (1) represents the probability density of having a trajectory with s jumps at $(t_1, t_1 + dt_1)$, ..., $(t_s, t_s + dt_s)$. When we need to highlight that the final time of the spin history is t, we may write X as $X(t)$. Seeking simplicity, in almost all equations we will not write the conditioning of all dynamic quantities on a given initial condition [for example, in (1) we have $\sigma(t_0) = \sigma_0$].

The probability density $Q(X)$ fulfills the following normalization relation:

$$1 = \sum_X^t Q^t(X) = \sum_{s=0}^{\infty} \int_{t_0}^t dt_1 \int_{t_1}^t dt_2 ... \times \int_{t_{s-1}}^t dt_s\, Q_s(t_0, t_1, ..., t_s, t|\sigma(t_0) = \sigma_0). \tag{2}$$

The sum $\sum_X^t$ in Eq. (2) goes over all histories that occur between t_0 and t, starting with $\sigma(t_0) = \sigma_0$. It is explicitly written on the right-hand side as a sum $\sum_{s=0}^{\infty}$ of time integrals. Each term of that sum corresponds to histories that have exactly s jumps, and the integrals account for all the possible jumping times $t_1, t_2, ..., t_s$.

Instantaneous magnitudes can be written as marginals of $Q^t(X)$. For example,

$$P^t(\sigma) = \sum_{X|\sigma(t)=\sigma}^t Q^t(X), \tag{3}$$

where the sum $\sum_{X|\sigma(t)=\sigma}^t$ goes over all the histories $X(t)$ such that $\sigma(t) = \sigma$ and can be written similarly as $\sum_X^t$ [see Eq. (2)]. In what follows, we will use the symbol $\sum_{X|\sigma}^t$ as a shortening of $\sum_{X|\sigma(t)=\sigma}^t$.

As we will show, some properties of the time evolution of magnitudes like $P^t(\sigma)$ can be obtained by working directly over $Q^t(X)$.

A. From random point processes to master equations

Master equations are a common instrument in the study of continuous-time dynamics. As a proof of the validity of the random point process approach, we will show its equivalence with the formulation of master equations in two examples: the time evolution of a single noninteracting variable and the dynamics of N-interacting spins. Through the derivations, the reader will become familiar with properties and procedures that will be used in Sec. III.

1. Single variable

The master equation for the time evolution a single spin without interactions reads

$$\frac{dP^t(\sigma)}{dt} = -r(\sigma)P^t(\sigma) + r(-\sigma)P^t(-\sigma), \tag{4}$$

where $r(\sigma)$ is the transition rate between the states σ and $-\sigma$.

To derive Eq. (4) from the TRPP, we will differentiate (3). Differentiation in this context should be handled carefully since increasing t means we are changing the sample space itself. Instead of using calculus rules to differentiate, we use

the definition of derivative as the limit of the incremental ratio:

$$\frac{dP^t(\sigma)}{dt} = \lim_{\Delta t \to 0} \frac{P^{t+\Delta t}(\sigma) - P^t(\sigma)}{\Delta t}. \tag{5}$$

For the sake of the discussion in the next sections, let us write down the calculations in detail.

Let us say that the final state of the trajectory X is $X(t) = \sigma$. Then the probability density $Q^t(X)$ can take the form [1,2]

$$Q^t(X) = r(\sigma_0)e^{-r(\sigma_0)(t_1-t_0)}r(-\sigma_0)e^{-r(-\sigma_0)(t_2-t_1)}\dots r(-\sigma)e^{-r(-\sigma)(t_s-t_{s-1})}e^{-r(\sigma)(t-t_s)}. \tag{6}$$

The right-hand side of Eq. (6) is the probability density of the waiting times of the history $X : [t_0, t] \to \{1, -1\}$, whose jumps occur at $(t_1, t_2, ..., t_s)$, with rates $r(\sigma)$.

Now we will write $P^{t+\Delta t}(\sigma)$ as the marginalization of $Q^{t+\Delta t}(X)$ and then expand to first order in Δt. Explicitly writing that marginalization as in Eq. (2):

$$P^{t+\Delta t}(\sigma) = \sum_s \int_{t_0}^{t+\Delta t} dt_1 \int_{t_1}^{t+\Delta t} dt_2 \dots \int_{t_{s-1}}^{t+\Delta t} dt_s\, Q^{t+\Delta t}(X). \tag{7}$$

Here, the sum on the right-hand side goes over all the values of the number of jumps (denoted as s) such that $X(t) = \sigma$.

Now we must keep only the order Δt term in (7). Let us expand first $Q^{t+\Delta t}(X)$ and leave the rest untouched. Equation (6) can be rearranged as

$$Q^{t+\Delta t}(X) = \left[\prod_{l=1}^{s} r(\sigma(t_l))\right] \exp\left\{-\int_{t_0}^{t+\Delta t} r(\sigma(\tau))d\tau\right\}, \tag{8}$$

where the jumps in the history X occur at the times t_l, with $l = 1, 2, \dots, s$.

In (8), the probability of having the last jump in the interval $[t, t + \Delta t]$ is $r(-\sigma)\Delta t$ and, more generally, the probability of occurrence of n jumps is proportional to $(\Delta t)^n$. Therefore, when Δt goes to zero, with probability 1 there are no jumps in $[t, t + \Delta t]$ and none of the times t_l belongs to that interval.

We can then expand the exponential in (8) and write

$$\begin{aligned} Q^{t+\Delta t}(X) &= \left[\prod_{l=1}^{s} r(\sigma(t_l))\right] \exp\left\{-\int_{t_0}^{t} r(\sigma(\tau))d\tau\right\}[1 - r(\sigma)\Delta t] + o(\Delta t), \\ Q^{t+\Delta t}(X) &= Q^t(X)\big[1 - r(\sigma)\Delta t\big] + o(\Delta t). \end{aligned} \tag{9}$$

On the other hand, the sum of iterated integrals in (7) is of order $(\Delta t)^s$ by itself. However, for each integral we have the property $\int_{t_0}^{t+\Delta t} d\tau = \int_{t_0}^{t} d\tau + \int_{t}^{t+\Delta t} d\tau$, and we can write

$$\sum_s \int_{t_0}^{t+\Delta t} dt_1 \int_{t_1}^{t+\Delta t} dt_2 \dots \int_{t_{s-1}}^{t+\Delta t} dt_s = \sum_s \int_{t_0}^{t} dt_1 \int_{t_1}^{t} dt_2 \dots \int_{t_{s-1}}^{t} dt_s + \sum_s \int_{t_0}^{t} dt_1 \int_{t_1}^{t} dt_2 \dots \int_{t}^{t+\Delta t} dt_s + o(\Delta t). \tag{10}$$

The first term of the right-hand side of (10) is an operator over the space of the histories that occur in the interval $[t_0, t]$. It can be safely applied to the expansion (9) of the probability density $Q^{t+\Delta t}(X)$ to give a contribution of order $O((\Delta t)^0) \equiv O(1)$,

$$I_0 = \sum_s \int_{t_0}^{t} dt_1 \int_{t_1}^{t} dt_2 \dots \int_{t_{s-1}}^{t} dt_s Q^t(X) = P^t(\sigma), \tag{11}$$

and a contribution of order $O(\Delta t)$:

$$I_1 = -\sum_s \int_{t_0}^{t} dt_1 \int_{t_1}^{t} dt_2 \dots \int_{t_{s-1}}^{t} dt_s Q^t(X)\, r(\sigma)\Delta t = -P^t(\sigma)\, r(\sigma)\Delta t. \tag{12}$$

Together, $I_0 + I_1$ represent the probability density of having $\sigma(t) = \sigma$ and no jumps in $[t, t + \Delta t]$.

In the second sum of (10), we have an operator that acts over the space where all jumps, except the last one, took place in $[t_0, t]$, and the last jump occurs in $[t, t + \Delta t]$. Therefore, we can obtain a second contribution of order $O(\Delta t)$ by applying this operator to the probability density Q of having only one jump in $[t, t + \Delta t]$. Remembering the parametrization (8) and expanding in powers of Δt:

$$\begin{aligned} I_2 &= \sum_s \int_{t_0}^{t} dt_1 \dots \int_{t_{s-2}}^{t} dt_{s-1} \left[\prod_{l=1}^{s-1} r(\sigma(t_l))\right] e^{-\int_{t_0}^{t} r(\sigma(\tau))d\tau} \int_{t}^{t+\Delta t} dt_s\, r(\sigma(t_s)) e^{-\int_{t}^{t+\Delta t} r(\sigma(\tau))d\tau}, \\ I_2 &= \left(\sum_s \int_{t_0}^{t} dt_1 \dots \int_{t_{s-2}}^{t} dt_{s-1} \left[\prod_{l=1}^{s-1} r(\sigma(t_l))\right] e^{-\int_{t_0}^{t} r(\sigma(\tau))d\tau}\right)(r(-\sigma)\Delta t) + o(\Delta t). \end{aligned} \tag{13}$$

In (13) we have used that, to fulfill the condition $\sigma(t) = \sigma$, the last jump must happen from $-\sigma$ to σ, with rate $r(-\sigma)$. The sum inside parenthesis in the equation now goes over all histories that end with $\sigma(t) = -\sigma$, and therefore is equal to $P^t(-\sigma)$. Thus $I_2 = P^t(-\sigma)\, r(-\sigma)\Delta t + o(\Delta t)$ represents the probability density of having $\sigma(t) = -\sigma$ and only one jump in $[t, t + \Delta t]$.

Putting all this together:

$$P^{t+\Delta t}(\sigma) = I_0 + I_1 + I_2 + o(\Delta t), \quad P^{t+\Delta t}(\sigma) = P^t(\sigma) - P^t(\sigma)\, r(\sigma)\Delta t + P^t(-\sigma)\, r(-\sigma)\Delta t + o(\Delta t). \tag{14}$$

By subtracting $P^t(\sigma)$ from both sides of (14), dividing by Δt and taking the limit $\Delta t \to 0$, we obtain the desired result (4):

$$\frac{dP^t(\sigma)}{dt} = -r(\sigma)P^t(\sigma) + r(-\sigma)P^t(-\sigma).$$

2. Multiple variables

In this case, where we have the time evolution of the N-interacting spins $\vec{\sigma} = \{\sigma_1, ..., \sigma_N\}$, the master equation is

$$\frac{dP^t(\vec{\sigma})}{dt} = -\sum_{i=1}^{N}[r_i(\vec{\sigma})P^t(\vec{\sigma}) - r_i(F_i[\vec{\sigma}])P^t(F_i[\vec{\sigma}])], \tag{15}$$

where $F_i[\vec{\sigma}]$ is an operator that transforms the state $\vec{\sigma} = \{\sigma_1, ..., \sigma_i, ..., \sigma_N\}$ into the state $F_i[\vec{\sigma}] = \{\sigma_1, ..., -\sigma_i, ..., \sigma_N\}$, and $r_i(\vec{\sigma})$ is the transition rate between $\vec{\sigma}$ and $F_i[\vec{\sigma}]$.

Similarly as in (3), the probability density $P^t(\vec{\sigma})$ is given by

$$P^t(\vec{\sigma}) = \sum_{\vec{X}|\vec{\sigma}}^{t} Q^t(\vec{X}), \tag{16}$$

where $\vec{X} = \{X_1, \ldots, X_N\}$ is the vector of the histories of all spins.

Now we must differentiate (16) similarly as with (3):

$$\frac{dP^t(\vec{\sigma})}{dt} = \lim_{\Delta t \to 0} \frac{P^{t+\Delta t}(\vec{\sigma}) - P^t(\vec{\sigma})}{\Delta t}. \tag{17}$$

The set of individual histories of N-interacting spins, $Q^t(\vec{X})$, can be written as a product of probability densities $\Phi_a^t(X_a|\vec{X}_{\setminus a})$ of the history X_a with the histories of all the other spins $\vec{X}_{\setminus a}$ fixed [23]:

$$Q^t(X_1, X_2, ..., X_N) = \prod_{i=1}^{N} \Phi_i^t(X_i|\vec{X}_{\setminus i}). \tag{18}$$

Each $\Phi_i^t(X_i|\vec{X}_{\setminus i})$ can be parametrized like in (8) [1,2]:

$$\Phi_i^t(X_i|\vec{X}_{\setminus i}) = \left[\prod_{l_i=1}^{s_i} r_i(\vec{\sigma}(t_{l_i}))\right] \exp\left\{-\int_{t_0}^{t} r_i(\vec{\sigma}(\tau))d\tau\right\}. \tag{19}$$

As before, we will write $P^{t+\Delta t}(\vec{\sigma})$ as the marginalization of $Q^{t+\Delta t}(\vec{X})$ and then expand to first order in Δt. Explicitly writing that marginalization as in (7):

$$P^{t+\Delta t}(\vec{\sigma}) = \sum_{s_1=0}^{\infty}\sum_{s_2=0}^{\infty}..\sum_{s_N=0}^{\infty}\left[\prod_{i=1}^{N}\int_{t_0}^{t+\Delta t} dt_1^i \int_{t_1^i}^{t+\Delta t} dt_2^i \ldots \int_{t_{s_i-1}^i}^{t+\Delta t} dt_{s_i}^i\right] Q^{t+\Delta t}(X_1, X_2, \ldots, X_N). \tag{20}$$

To expand $Q^{t+\Delta t}(\vec{X})$ requires expanding each $\Phi_i^{t+\Delta t}(X_i|\vec{X}_{\setminus i})$, which is almost the same we did in (9):

$$\Phi_i^{t+\Delta t}(X_i|\vec{X}_{\setminus i}) = \Phi_i^t(X_i|\vec{X}_{\setminus i})\,[1 - r_i(\vec{\sigma}(t))\,\Delta t] + o(\Delta t). \tag{21}$$

Thus,

$$Q^{t+\Delta t}(\vec{X}) = \prod_{i=1}^{N} \Phi_i^{t+\Delta t}(X_i|\vec{X}_{\setminus i}), \quad Q^{t+\Delta t}(\vec{X}) = \prod_{i=1}^{N} \Phi_i^t(X_i|\vec{X}_{\setminus i})\left[1 - \Delta t \sum_{k=1}^{N} r_k(\vec{\sigma}(t))\right] + o(\Delta t),$$

$$Q^{t+\Delta t}(\vec{X}) = Q^t(\vec{X})\left[1 - \Delta t \sum_{k=1}^{N} r_k(\vec{\sigma}(t))\right] + o(\Delta t). \tag{22}$$

Similarly, as with (11) and (12), we will use (22) to get two contributions of order $O(1)$ and $O(\Delta t)$, respectively:

$$I_0 = \sum_{s_1=0}^{\infty}\cdots\sum_{s_N=0}^{\infty}\left[\prod_{i=1}^{N}\int_{t_0}^{t} dt_1^i \ldots \int_{t_{s_i-1}^i}^{t} dt_{s_i}^i\right] Q^t(\vec{X}) = P^t(\vec{\sigma}), \tag{23}$$

$$I_1 = \left(\sum_{s_1=0}^{\infty}\cdots\sum_{s_N=0}^{\infty}\left[\prod_{i=1}^{N}\int_{t_0}^{t} dt_1^i \ldots \int_{t_{s_i-1}^i}^{t} dt_{s_i}^i\right] Q^t(\vec{X})\right)\left(-\Delta t\sum_{k=1}^{N} r_k(\vec{\sigma}(t))\right), \quad I_1 = -P^t(\vec{\sigma})\,\Delta t\sum_{k=1}^{N} r_k(\vec{\sigma}(t)). \tag{24}$$

As in (10), we can split the sum of iterated integrals on the right-hand side of (20) to get $O(\Delta t)$ contributions. The latter is an operator that acts over the space of the histories where one and only one spin jumps in $[t, t+\Delta t]$. The rest is a calculation essentially equal to the one in (13):

$$\begin{aligned} I_2 = &\sum_{k=1}^{N}\sum_{s_1=0}^{\infty}\cdots\sum_{s_N=0}^{\infty}\left[\prod_{i\neq k}\int_{t_0}^{t} dt_1^i \ldots \int_{t_{s_i-1}^i}^{t} dt_{s_i}^i\right]\int_{t_0}^{t} dt_1^k \ldots \int_{t_{s_k-2}}^{t} dt_{s_k-1}^k\left[\prod_{i\neq k}\Phi_i^t(X_i|\vec{X}_{\setminus i})\right] \\ &\times\left[\prod_{l_k=1}^{s_k-1} r_k(\vec{\sigma}(t_{l_k}))\right] e^{-\int_{t_0}^{t} r_k(\vec{\sigma}(\tau))d\tau} r_k(F_k[\vec{\sigma}(t)])\Delta t + o(\Delta t), \\ I_2 = &\sum_{k=1}^{N} P^t(F_k[\vec{\sigma}])\, r_k(F_k[\vec{\sigma}(t)])\,\Delta t. \end{aligned} \tag{25}$$

Finally, the expansion of $P^{t+\Delta t}(\vec{\sigma})$ gives

$$\begin{aligned} &P^{t+\Delta t}(\vec{\sigma}) = I_0 + I_1 + I_2 + o(\Delta t), \\ &P^{t+\Delta t}(\vec{\sigma}) = P^t(\vec{\sigma}) - \Delta t\sum_{k=1}^{N} P^t(\vec{\sigma}) r_k(\vec{\sigma}) + \Delta t\sum_{k=1}^{N} P^t(F_k[\vec{\sigma}]) r_k(F_k[\vec{\sigma}]) + o(\Delta t), \end{aligned} \tag{26}$$

and using (17) we obtain the usual master equation [1] for a set of N-interacting spins (15):

$$\frac{dP^t(\vec{\sigma})}{dt} = -\sum_{i=1}^{N}[r_i(\vec{\sigma})P^t(\vec{\sigma}) - r_i(F_i[\vec{\sigma}])P^t(F_i[\vec{\sigma}])]. \tag{27}$$

Unfortunately, to solve (27), even numerically, is in general a very difficult task because the densities $P^t(\vec{\sigma})$ are high dimensional objects.

III. HIERARCHICAL CAVITY MASTER EQUATIONS

This section contains the main analytical contribution of our paper. We will exploit techniques similar to the ones presented above to write down a set of closed differential equations for the stochastic dynamics of discrete variables in a random graph. We generalize a closure presented in Ref. [5] substituting an uncontrolled approximation by new equations derived from first principles through the TRPP.

To simplify the reading, this section is divided in five subsections. In Sec. III A, we introduce the dynamic cavity method to study systems defined over treelike graphs. In Sec. III B, we use that formulation to write the local probability densities sitting on any group of connected nodes in terms of dynamic cavity messages. Then we derive the known local master equations for those probability densities. In Sec. III C, we repeat the same procedure to obtain analogous equations for cavity probability densities. A general approximated method for closing these equations is presented and discussed in Sec. III D. There, we show how these closed dynamic equations can be organized in a system of hierarchical approximations.

A. Treelike architecture and cavity messages

In this subsection, we will introduce the dynamic cavity messages for treelike graphs. Now, every spin σ_i interacts only with the spins sitting in its neighborhood: $\sigma_{\partial i}$ (the symbol ∂i denotes the set of nodes in the neighborhood of i). Therefore, our stochastic process involves flipping rates r_i that depend only on σ_i and $\sigma_{\partial i}$.

In this scenario, it is possible to separate the spins into two disconnected networks just by removing a single connection between two nodes. We first select a spin, say i, and rewrite Eq. (18) following the treelike structure around it:

$$\begin{aligned} Q^t(X_1,\ldots,X_N) = \Phi_i^t(X_i|X_{\partial i})\prod_{k\in\partial i}\Bigg[\Phi_k^t(X_k|X_{\partial k})\prod_{m\in\partial k\setminus i} \\ \times\left(\Phi_k^t(X_m|X_{\partial m})\prod_{l\in\partial m\setminus k}\ldots\right)\Bigg]. \end{aligned} \tag{28}$$

Those are the only spins that directly interact with i and therefore we adapted the previous notation of the Φ probability densities. The symbol $X_{\partial i}$ represents the set of histories of the nodes in ∂i. Furthermore, let $G_k^{(i)}$ be the subgraph expanded from the site k after removing the link (ik). Let us define $\{X\}_{ik}$ as the set of histories related to the spins included in $G_k^{(i)}$ except for X_k. Now we can express (28) as

$$Q^t(X_1,\ldots,X_N) = \Phi_i^t(X_i|X_{\partial i})\prod_{k\in\partial i} M_{ki}^t(X_i, X_k, \{X\}_{ik}). \tag{29}$$

Here M_{ki}^t is just a shortening for the expression inside brackets. Marginalizing Q on all histories except $X_i, X_{\partial i}$,

we get

$$Q^t(X_i, X_{\partial i}) = \Phi_i^t(X_i|X_{\partial i}) \prod_{k\in\partial i} \mu^t_{k\to(ki)}(X_k|X_i). \quad (30)$$

The new functions $\mu^t_{k\to(ki)}(X_k|X_i)$, called dynamic cavity messages, are the marginals:

$$\mu^t_{k\to(ki)}(X_k|X_i) = \sum_{\{X\}_{ik}}^{t} M^t_{ki}(X_i, X_k, \{X\}_{ik}). \quad (31)$$

It can be shown that $\mu^t_{k\to(ki)}(X_k|X_i)$ can be properly normalized to one, and it is convenient to do so. Each cavity message has the interpretation of the probability density of history X_k given X_i fixed.

If we now take two neighbors, i and j, and make a similar reasoning, we conclude that their marginal probability density can be written as

$$Q^t(X_i, X_j) = \mu^t_{i\to(ij)}(X_i|X_j)\mu^t_{j\to(ji)}(X_j|X_i). \quad (32)$$

These cavity messages can be parametrized as other similar dynamical quantities [see Eqs. (6) and (19)]:

$$\begin{aligned}\mu^t_{i\to(ij)}(X_i|X_j) = {} & \lambda_{i\to(ij)}(X_i, X_j, t_0)\, e^{-\int_{t_0}^{t_1}\lambda_i^\tau d\tau} \\ & \times \lambda_{i\to(ij)}(X_i, X_j, t_1) e^{-\int_{t_1}^{t_2}\lambda_i^\tau d\tau} \\ & \times \cdots \times \lambda_{i\to(ij)}(X_i, X_j, t_{s_i}) e^{-\int_{t_{s_i}}^{t}\lambda_i^\tau d\tau}, \end{aligned} \quad (33)$$

only that now the jumps occur with unknown rates $\lambda_{i\to(ij)}(X_i, X_j, t)$, which in general are functions of the full histories X_i and X_j taken from t_0 to t.

Then, as in (21) we can expand Φ and μ to order Δt (for the latter, see Appendix B):

$$\begin{aligned}&\Phi_i^{t+\Delta t}(X_i|X_{\partial i}) \\ &\quad = \Phi_i^t(X_i|X_{\partial i})\,[1 - r_i(\sigma_i(t), \sigma_{\partial i}(t))\,\Delta t] + o(\Delta t), \end{aligned} \quad (34)$$

$$\begin{aligned}&\mu^{t+\Delta t}_{i\to(ij)}(X_i|X_j) \\ &\quad = \mu^t_{i\to(ij)}(X_i|X_j)\,[1 - \lambda_{i\to(ij)}(X_i, X_j, t)\Delta t] + o(\Delta t). \end{aligned} \quad (35)$$

Equations (31)–(35) were already present in Ref. [5], but they will also be at the basis of our derivation. They will be exploited below to write a more general set of equations than the ones presented in Ref. [5].

B. Equations for local probability densities

In this subsection, we further explore the connection between the TRPP and masterlike equations, now exploiting a message-passing formalism usually found when studying problems in treelike graphs. Although the final equation to be obtained can be deduced using simpler techniques, we believe that the approach presented here has a pedagogical value and will clarify the methodology used in Sec. III C to obtain more original results.

By eliminating a group of connected nodes from a treelike graph, we always divide it into several treelike subgraphs. We illustrate this in the top-left panel of Fig. 1. There, we colored in gray the subtrees obtained after removing the white nodes in the center. As we learned in Sec. III A, if we marginalize the full distribution $Q^t(\vec{X})$ over all the histories in these gray subgraphs, we obtain the probability density of the set of histories corresponding to the connected group we have selected.

Therefore, if we denote the central node in the top-left panel of Fig. 1 by i, and remembering the steps from (28) to (30), we have

$$\begin{aligned}Q^t(\vec{X}_{\text{connected set}}) &= \sum_{\vec{X}_{\text{gray nodes}}}^{t} Q^t(\vec{X}), \\ Q^t(X_i, X_{\partial i}) &= \Phi_i^t(X_i|X_{\partial i}) \prod_{k\in\partial i} \mu^t_{k\to(ki)}(X_k|X_i). \end{aligned} \quad (36)$$

This procedure can be easily generalized to write any local probability density of the histories of a connected set of nodes. We just have to recognize inner and outer nodes: the first ones have all their neighbors belonging to the connected set and the second ones have at least one neighbor outside the connected set. The top-right and the bottom-left panels of Fig. 1 show examples of connected sets. In each case, we have a group of inner nodes (in white) and a group of outer nodes (in black).

The probability density of a connected set is always a marginal of the full probability density. However, to avoid a more involved analysis, we will separate the connected sets into two categories. A connected set is *of the first kind* when all its outer nodes have only one neighbor inside the set, and is *of the second kind* when at least one outer node has more than one neighbor inside the set. This distinction is important because in the first case we can directly write the corresponding probability density as a product of local weights Φ and dynamic cavity messages μ. We must simply include a local weight for each inner node and a cavity message for each outer node.

For example, the probability density corresponding to the connected set in the top-right panel of Fig. 1 is

$$\begin{aligned}&Q^t(\vec{X}_{\text{connected set}}) = \sum_{\vec{X}_{\text{gray nodes}}}^{t} Q^t(\vec{X}), \\ &Q^t(X_i, X_{\partial i}, X_{\partial k\setminus i}, X_{\partial l\setminus i}) \\ &\quad = \Phi_i^t(X_i|X_{\partial i}) \left[\prod_{m\in\partial i\setminus j} \Phi^t_m(X_m|X_{\partial m})\right] \mu^t_{j\to(ji)}(X_j|X_i) \\ &\qquad \times \left[\prod_{n\in\partial k\setminus i} \mu^t_{n\to(nk)}(X_n|X_k)\right]\left[\prod_{n\in\partial l\setminus i} \mu^t_{n\to(nl)}(X_n|X_l)\right], \end{aligned} \quad (37)$$

where $j, k, l \in \partial i$. A representation of this product of Φ and μ functions is shown in the bottom-right panel of Fig. 1.

Connected sets of the second kind do not require a different treatment. Fortunately, we can always add nodes to convert these into sets of the first kind. For example, we can transform the bottom-left panel of Fig. 1 into the top-right panel just by adding node l_1 to the connected set. Then we can simply compute a

$$Q^t\left(X_i, X_{\partial i}, X_{\partial k\setminus i}, X_{l_2}\right) = \sum_{X_{l_1}}^{t} Q^t\left(X_i, X_{\partial i}, X_{\partial k\setminus i}, X_{l_1}, X_{l_2}\right). \quad (38)$$

Thus, the probability density of any set of the second kind can be written as a marginal of the probability density of a set of the first kind just like (38) is written in terms of (37).

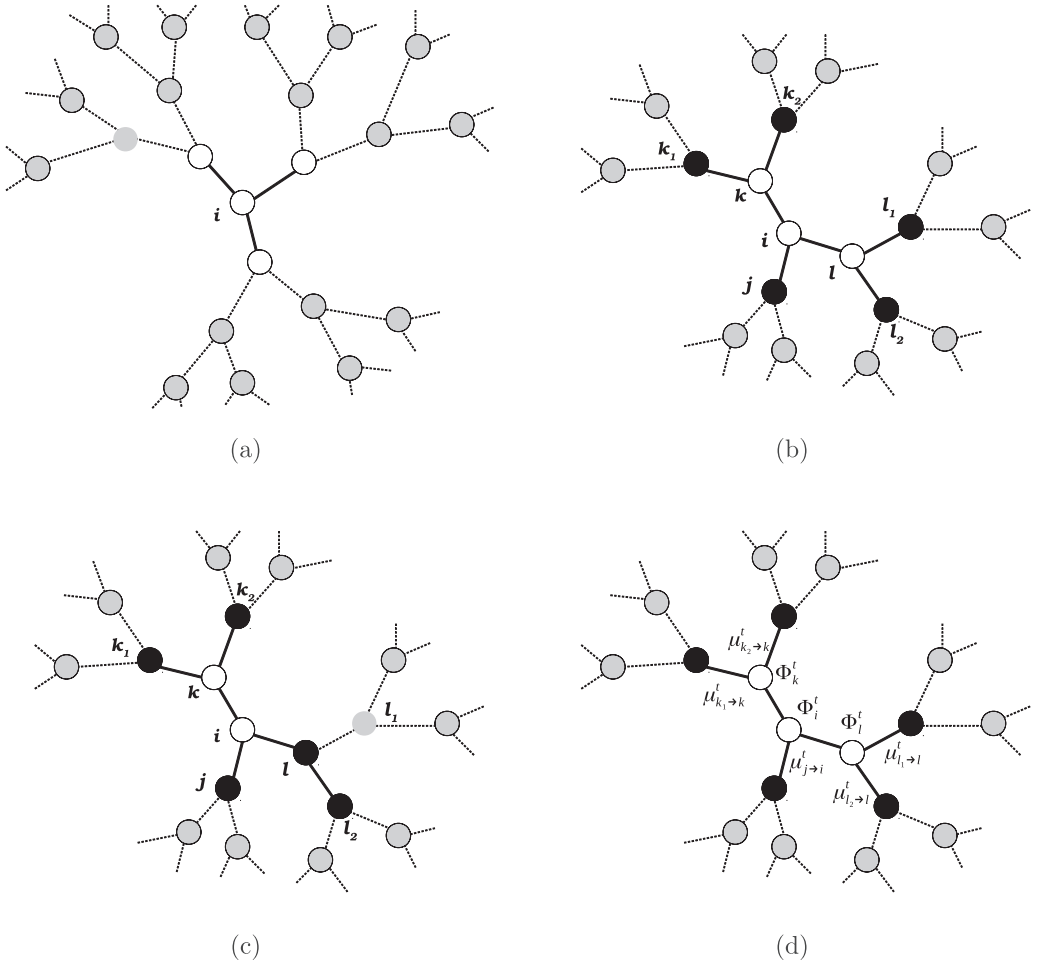

FIG. 1. (a) Selection of a connected set with four nodes (white) from a treelike graph. The full graph is divided in six treelike subgraphs (gray nodes). (b) Dividing a connected set with eight nodes in two groups: inner (white) and outer nodes (black). This is a connected set of the first kind, because every outer node has only one neighbor inside the set. (c) Connected set with seven nodes. According to our classification, the connected set is of the second kind because node l has two neighbors, i and l_2, which belong to the set. (d) Local weights and cavity messages present in the probability densities related to the connected set shown in top-right panel.

To derive a differential equation for the time evolution of any instantaneous local probability density P^t, we should concentrate on connected sets of the first kind. To fix ideas, let us work with such a connected set containing n inner nodes and m outer nodes. We will say that the sets $\mathcal{I} = \{i_1, i_2, \ldots, i_n\}$ and $\mathcal{O} = \{o_1, o_2, \ldots, o_m\}$ contain the inner and outer nodes, respectively. Furthermore, we can define a function $\varphi : \mathcal{O} \to \mathcal{I}$ that gives, for every outer node o_k, the corresponding inner node $\varphi(o_k)$. Let us use the notation $\varphi(o_k) \equiv \varphi_k$ to simplify the writing of the following equations.

The instantaneous probability density can be written as

$$P^t(\vec{\sigma}_{\mathcal{O}}, \vec{\sigma}_{\mathcal{I}}) = \sum_{\vec{X}_{\mathcal{I}}|\vec{\sigma}_{\mathcal{I}}}^{t} \sum_{\vec{X}_{\mathcal{O}}|\vec{\sigma}_{\mathcal{O}}}^{t} Q^t(\vec{X}_{\mathcal{O}}, \vec{X}_{\mathcal{I}}), \tag{39}$$

where $\vec{\sigma}_{\mathcal{I}}$ and $\vec{\sigma}_{\mathcal{O}}$ are the vectors of the instantaneous states of the inner and outer nodes, respectively, and $\vec{X}_{\mathcal{I}}$ and $\vec{X}_{\mathcal{O}}$ are the corresponding vectors of the histories of those nodes. On the other hand,

$$Q^t(\vec{X}_{\mathcal{O}}, \vec{X}_{\mathcal{I}}) = \left[\prod_{k=1}^{m} \mu^t_{o_k \to (o_k \varphi_k)}\left(X_{o_k}\middle|X_{\varphi_k}\right)\right]\left[\prod_{k=1}^{n} \Phi^t_{i_k}\left(X_{i_k}\middle|X_{\partial i_k}\right)\right], \tag{40}$$

where

Now we need to expand (39) to order Δt. As in Sec. II A we can write an order Δt expression for $Q^{t+\Delta t}(\vec{X}_{\mathcal{O}}, \vec{X}_{\mathcal{I}})$. Remembering (34) and (35), we have

$$Q^{t+\Delta t}(\vec{X}_{\mathcal{O}}, \vec{X}_{\mathcal{I}}) = \left[\prod_{k=1}^{m} \mu^t_{o_k \to \varphi_k}\left[1 - \lambda^t_{o_k \to \varphi_k}\Delta t\right] + o(\Delta t)\right]\left[\prod_{k=1}^{n} \Phi^t_{i_k}\left[1 - r^t_{i_k}\,\Delta t\right] + o(\Delta t)\right],$$

$$Q^{t+\Delta t}(\vec{X}_{\mathcal{O}}, \vec{X}_{\mathcal{I}}) = Q^t(\vec{X}_{\mathcal{O}}, \vec{X}_{\mathcal{I}}) - \Delta t \sum_{l=1}^{n} r^t_{il}\left[\prod_{k=1}^{m} \mu^t_{o_k \to \varphi_k}\right]\left[\prod_{k=1}^{n} \Phi^t_{i_k}\right] - \Delta t \sum_{l=1}^{m} \lambda^t_{o_l \to \varphi_l}\left[\prod_{k=1}^{m} \mu^t_{o_k \to \varphi_k}\right]\left[\prod_{k=1}^{n} \Phi^t_{i_k}\right], \tag{41}$$

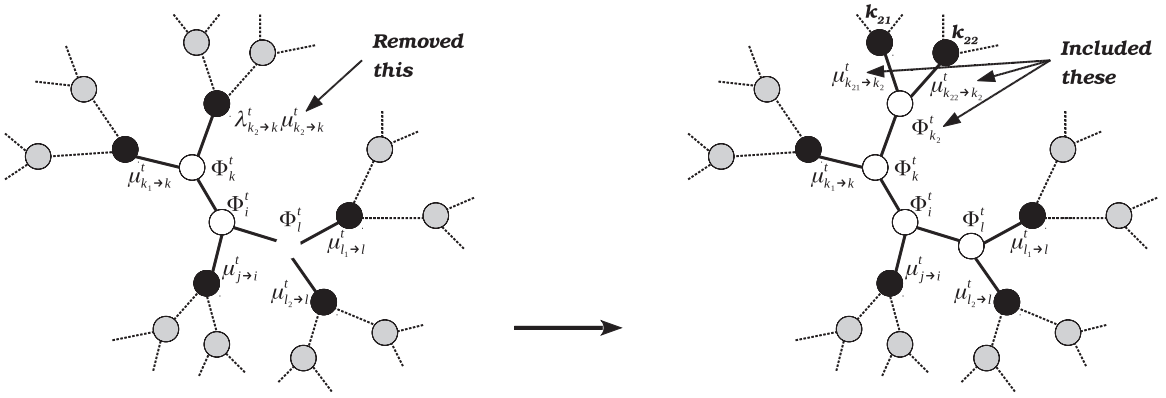

FIG. 2. This figure illustrates what happens when we apply the relation (46) to Eq. (47) in the particular case of the connected set of the right panels of Fig. 1. We took the outer node k_2 (see Fig. 1) as o_l. After including a new local weight $\Phi^t_{k_2}$ and two new messages $\mu^t_{k_{21}\to k_2}$ and $\mu^t_{k_{21}\to k_2}$, we end up having the probability density of a bigger connected set that includes all neighbors of k_2.

where we have shortened our notation as follows:

$$\Phi^t_{i_k}\left(X_{i_k}\middle|X_{\partial i_k}\right)\equiv\Phi^t_{i_k},\quad \mu^t_{o_k\to(o_k\varphi_k)}\left(X_{o_k}\middle|X_{i_k}\right)\equiv\mu^t_{o_k\to\varphi_k},$$
$$r_{i_k}\left(\sigma_{i_k}(t),\sigma_{\partial i_k}(t)\right)\equiv r^t_{i_k},\quad \lambda_{o_k\to(o_k\varphi_k)}\left(X_{o_k},X_{i_k},t\right)\equiv\lambda^t_{o_k\to\varphi_k}. \tag{42}$$

Similarly as before, there are three contributions to the expansion of (39) to order Δt:

$$I_0=\sum_{\vec{X}_{\mathcal{O}}|\vec{\sigma}_{\mathcal{O}}}^{t}\sum_{\vec{X}_{\mathcal{I}}|\vec{\sigma}_{\mathcal{I}}}^{t}Q^t(\vec{X}_{\mathcal{O}},\vec{X}_{\mathcal{I}})=P^t(\vec{\sigma}_{\mathcal{O}},\vec{\sigma}_{\mathcal{I}}), \tag{43}$$

$$I_1=-\Delta t\sum_{\vec{X}_{\mathcal{O}}|\vec{\sigma}_{\mathcal{O}}}^{t}\sum_{\vec{X}_{\mathcal{I}}|\vec{\sigma}_{\mathcal{I}}}^{t}\left[\prod_{k=1}^{m}\mu^t_{o_k\to\varphi_k}\right]\left[\prod_{k=1}^{n}\Phi^t_{i_k}\right]\left[\sum_{l=1}^{n}r^t_{i_l}+\sum_{l=1}^{m}\lambda^t_{o_l\to\varphi_l}\right], \tag{44}$$

$$I_2=\Delta t\sum_{l=1}^{n}\sum_{\vec{X}_{\mathcal{O}}|\vec{\sigma}_{\mathcal{O}}}^{t}\sum_{\vec{X}_{\mathcal{I}}|F_{i_l}[\vec{\sigma}_{\mathcal{I}}]}^{t}\left[\prod_{k=1}^{m}\mu^t_{o_k\to\varphi_k}\right]\left[\prod_{k=1}^{n}\Phi^t_{i_k}\right]r^t_{i_l}+\Delta t\sum_{l=1}^{m}\sum_{\vec{X}_{\mathcal{O}}|F_{o_l}[\vec{\sigma}_{\mathcal{O}}]}^{t}\sum_{\vec{X}_{\mathcal{I}}|\vec{\sigma}_{\mathcal{I}}}^{t}\left[\prod_{k=1}^{m}\mu^t_{o_k\to\varphi_k}\right]\left[\prod_{k=1}^{n}\Phi^t_{i_k}\right]\lambda^t_{o_l\to\varphi_l}. \tag{45}$$

In Appendix B [see Eq. (B12)], we derive the identity

$$\lambda^t_{i\to j}\ \mu^t_{i\to j}=\sum_{X_{\partial i\setminus j}}^{t}r^t_i\,\Phi^t_i\prod_{k\in\partial i\setminus j}\mu^t_{k\to i}, \tag{46}$$

which leads to

$$\left[\prod_{k=1}^{m}\mu^t_{o_k\to\varphi_k}\right]\left[\prod_{k=1}^{n}\Phi^t_{i_k}\right]\lambda^t_{o_l\to\varphi_l}=\left[\prod_{\substack{k=1\\k\neq l}}^{m}\mu^t_{o_k\to\varphi_k}\right]\left[\prod_{k=1}^{n}\Phi^t_{i_k}\right]\lambda^t_{o_l\to\varphi_l}\ \mu^t_{o_l\to\varphi_l}, \tag{47}$$

$$\left[\prod_{k=1}^{m}\mu^t_{o_k\to\varphi_k}\right]\left[\prod_{k=1}^{n}\Phi^t_{i_k}\right]\lambda^t_{o_l\to\varphi_l}=\left[\prod_{\substack{k=1\\k\neq l}}^{m}\mu^t_{o_k\to\varphi_k}\right]\left[\prod_{k=1}^{n}\Phi^t_{i_k}\right]\sum_{X_{\partial o_l\setminus\varphi_l}}^{t}r^t_{o_l}\,\Phi^t_{o_l}\left[\prod_{k\in\partial o_l\setminus\varphi_l}\mu^t_{k\to o_l}\right],$$

$$\left[\prod_{k=1}^{m}\mu^t_{o_k\to\varphi_k}\right]\left[\prod_{k=1}^{n}\Phi^t_{i_k}\right]\lambda^t_{o_l\to\varphi_l}=\sum_{X_{\partial o_l\setminus\varphi_l}}^{t}r^t_{o_l}\left[\prod_{\substack{k=1\\k\neq l}}^{m}\mu^t_{o_k\to\varphi_k}\right]\left[\prod_{k=1}^{n}\Phi^t_{i_k}\right]\Phi^t_{o_l}\left[\prod_{k\in\partial o_l\setminus\varphi_l}\mu^t_{k\to o_l}\right]. \tag{48}$$

Now, what does the product $[\prod_{\substack{k=1\\k\neq l}}^{m}\mu^t_{o_k\to\varphi_k}][\prod_{k=1}^{n}\Phi^t_{i_k}]\Phi^t_{o_l}[\prod_{k\in\partial o_l\setminus\varphi_l}\mu^t_{k\to o_l}]$ on the right-hand side of (48) stand for? As in the example of Fig. 2, we took (47) and removed the factor $\lambda^t_{o_l\to\varphi_l}\ \mu^t_{o_l\to\varphi_l}$. Then, we included a local weight, $\Phi^t_{o_l}$, and a group

of cavity messages $\mu^t_{k\to o_l}$. Therefore, in (48) we have all the local weights and cavity messages that appear in the probability density of a bigger connected set, which now includes all the neighbors of o_l.

Equation (48) transforms into

$$\left[\prod_{k=1}^{m}\mu^t_{o_k\to\varphi_k}\right]\left[\prod_{k=1}^{n}\Phi^t_{i_k}\right]\lambda^t_{o_l\to\varphi_l}=\sum_{X_{\partial o_l\setminus\varphi_l}}^{t} r^t_{o_l}\,Q^t\big(X_{\partial o_l\setminus\varphi_l},\vec{X}_{\mathcal{O}},\vec{X}_{\mathcal{I}}\big). \tag{49}$$

Thus, we can rewrite (44) and (45) to get

$$I_1=-\Delta t\sum_{\vec{X}_{\mathcal{O}}|\vec{\sigma}_{\mathcal{O}}}^{t}\sum_{\vec{X}_{\mathcal{I}}|\vec{\sigma}_{\mathcal{I}}}^{t}\left[\sum_{l=1}^{n} r^t_{i_l}Q^t(\vec{X}_{\mathcal{O}},\vec{X}_{\mathcal{I}})+\sum_{l=1}^{m}\sum_{X_{\partial o_l\setminus\varphi_l}}^{t} r^t_{o_l}\,Q\big(X_{\partial o_l\setminus\varphi_l},\vec{X}_{\mathcal{O}},\vec{X}_{\mathcal{I}}\big)\right],$$

$$I_1=-\Delta t\left[\sum_{l=1}^{n} r_{i_l}\big(\sigma_{i_l},\sigma_{\partial i_l}\big)P^t\big(\vec{\sigma}_{\mathcal{O}},\vec{\sigma}_{\mathcal{I}}\big)+\sum_{l=1}^{m}\sum_{\sigma_{\partial o_l\setminus\varphi_l}} r_{o_l}\big(\sigma_{o_l},\sigma_{\partial o_l}\big)P^t\big(\sigma_{\partial o_l\setminus\varphi_l},\vec{\sigma}_{\mathcal{O}},\vec{\sigma}_{\mathcal{I}}\big)\right], \tag{50}$$

$$I_2=\Delta t\sum_{l=1}^{n}\sum_{\vec{X}_{\mathcal{O}}|\vec{\sigma}_{\mathcal{O}}}^{t}\sum_{\vec{X}_{\mathcal{I}}|F_{i_l}[\vec{\sigma}_{\mathcal{I}}]}^{t} r^t_{i_l}\,Q(\vec{X}_{\mathcal{O}},\vec{X}_{\mathcal{I}})+\Delta t\sum_{l=1}^{m}\sum_{\vec{X}_{\mathcal{O}}|F_{o_l}[\vec{\sigma}_{\mathcal{O}}]}^{t}\sum_{\vec{X}_{\mathcal{I}}|\vec{\sigma}_{\mathcal{I}}}^{t} r^t_{o_l}\,Q(X_{\partial o_l\setminus\varphi_l},\vec{X}_{\mathcal{O}},\vec{X}_{\mathcal{I}}),$$

$$I_2=\Delta t\left[\sum_{l=1}^{n} r_{i_l}\big(-\sigma_{i_l},\sigma_{\partial i_l}\big)P^t\big(\vec{\sigma}_{\mathcal{O}},F_{i_l}[\vec{\sigma}_{\mathcal{I}}]\big)+\sum_{l=1}^{m}\sum_{\sigma_{\partial o_l\setminus\varphi_l}} r_{o_l}\big(-\sigma_{o_l},\sigma_{\partial o_l}\big)P^t\big(\sigma_{\partial o_l\setminus\varphi_l},F_{o_l}[\vec{\sigma}_{\mathcal{O}}],\vec{\sigma}_{\mathcal{I}}\big)\right], \tag{51}$$

where we have returned to the longer notation for the rates r^t_i [see Eq. (42)].

Putting (43), (50), and (51) together:

$$P^{t+\Delta t}(\vec{\sigma}_{\mathcal{O}},\vec{\sigma}_{\mathcal{I}})=I_0+I_1+I_2+o(\Delta t),$$

$$\begin{aligned}P^{t+\Delta t}(\vec{\sigma}_{\mathcal{O}},\vec{\sigma}_{\mathcal{I}})=P^t(\vec{\sigma}_{\mathcal{O}},\vec{\sigma}_{\mathcal{I}})&-\Delta t\sum_{l=1}^{n}\Big[r_{i_l}\big(\sigma_{i_l},\sigma_{\partial i_l}\big)P^t(\vec{\sigma}_{\mathcal{O}},\vec{\sigma}_{\mathcal{I}})-r_{i_l}\big(-\sigma_{i_l},\sigma_{\partial i_l}\big)P^t\big(\vec{\sigma}_{\mathcal{O}},F_{i_l}[\vec{\sigma}_{\mathcal{I}}]\big)\Big]\\&-\Delta t\sum_{l=1}^{m}\sum_{\sigma_{\partial o_l\setminus\varphi_l}} r_{o_l}\big(\sigma_{o_l},\sigma_{\partial o_l}\big)P^t\big(\sigma_{\partial o_l\setminus\varphi_l},\vec{\sigma}_{\mathcal{O}},\vec{\sigma}_{\mathcal{I}}\big)+\Delta t\sum_{l=1}^{m}\sum_{\sigma_{\partial o_l\setminus\varphi_l}} r_{i_l}\big(-\sigma_{i_l},\sigma_{\partial i_l}\big)P^t\big(\sigma_{\partial o_l\setminus\varphi_l},F_{o_l}[\vec{\sigma}_{\mathcal{O}}],\vec{\sigma}_{\mathcal{I}}\big)+o(\Delta t),\end{aligned} \tag{52}$$

and, finally,

$$\begin{aligned}\frac{dP^t(\vec{\sigma}_{\mathcal{O}},\vec{\sigma}_{\mathcal{I}})}{dt}=&-\sum_{l=1}^{n}\Big[r_{i_l}\big(\sigma_{i_l},\sigma_{\partial i_l}\big)P^t(\vec{\sigma}_{\mathcal{O}},\vec{\sigma}_{\mathcal{I}})-r_{i_l}\big(-\sigma_{i_l},\sigma_{\partial i_l}\big)P^t\big(\vec{\sigma}_{\mathcal{O}},F_{i_l}[\vec{\sigma}_{\mathcal{I}}]\big)\Big]\\&-\sum_{l=1}^{m}\sum_{\sigma_{\partial o_l\setminus\varphi_l}}\Big[r_{o_l}(\sigma_{o_l},\sigma_{\partial o_l})P^t\big(\sigma_{\partial o_l\setminus\varphi_l},\vec{\sigma}_{\mathcal{O}},\vec{\sigma}_{\mathcal{I}}\big)-r_{o_l}\big(-\sigma_{o_l},\sigma_{\partial o_l}\big)P^t\big(\sigma_{\partial o_l\setminus\varphi_l},F_{o_l}[\vec{\sigma}_{\mathcal{O}}],\vec{\sigma}_{\mathcal{I}}\big)\Big].\end{aligned} \tag{53}$$

Equation (53) is like a master equation for the combined set of variables $\{\vec{\sigma}_{\mathcal{O}},\vec{\sigma}_{\mathcal{I}}\}$, but it has a very peculiar structure. The first sum represents the contribution to the derivative due to flipping rates of spins sitting at inner nodes, and the second and third lines are the contribution related to outer nodes. Precisely, there we can notice that the time derivative of $P^t(\vec{\sigma}_{\mathcal{O}},\vec{\sigma}_{\mathcal{I}})$ depends on probability densities defined over bigger connected sets: $P^t(\sigma_{\partial o_l\setminus\varphi_l},\vec{\sigma}_{\mathcal{O}},\vec{\sigma}_{\mathcal{I}})$. This means that this is not a closed system of equations, and we need to complement it with other relations to obtain the time dependence of its variables.

Summarizing, in this subsection we presented a general method to obtain the exact differential equation of any local probability density for a treelike graph exploiting the TRPP. As we already mentioned, this equation can be derived through much simpler procedures and in more general contexts (see Appendix A for an example). However, we believe that the technique introduced here, and, in particular, the use of functions that act as *messages* may clarify the path to be followed in the next section.

C. Equations for cavity probability densities

To proceed further, it is necessary to find a way to close the set of equations (53). To do this, we need to first introduce a new set of masterlike equations. They will represent CMEs to be solved separately. With them, we may write $P^t(\sigma_{\partial o_l\setminus\varphi_l},\vec{\sigma}_{\mathcal{O}},\vec{\sigma}_{\mathcal{I}})$ in terms of the quantities $P^t(\vec{\sigma}_{\mathcal{O}},\vec{\sigma}_{\mathcal{I}})$ (see below), therefore closing the full system.

We start from the idea that, in a treelike graph, any local probability density Q of the histories of a connected set can

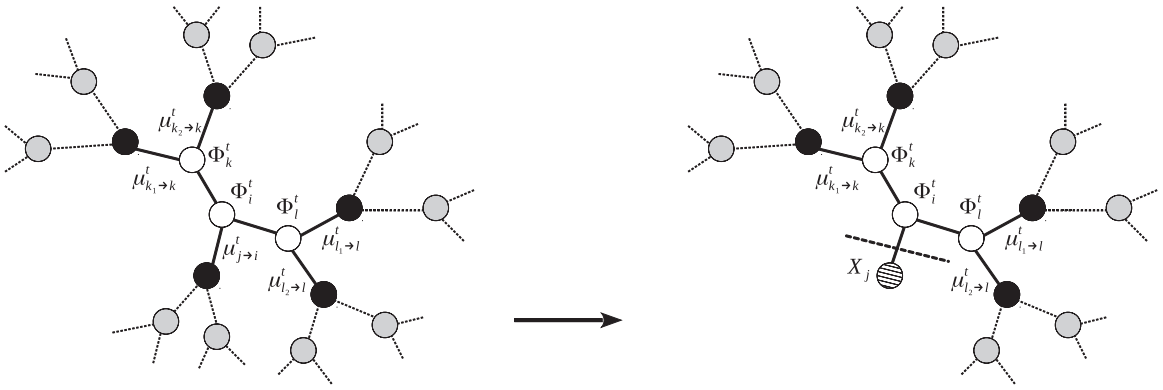

FIG. 3. This figure illustrates the relation between probability densities Q (left panel) and cavity probability densities q (right panel) defined over connected sets. In this case, q is obtained by removing the cavity message $\mu^t_{j\to i}$, and we say that q is defined in the cavity where X_j is fixed.

be written as

$$Q^t(\vec{X}_{\mathcal{O}},\vec{X}_{\mathcal{I}}) = \left[\prod_{k=1}^{m}\mu^t_{o_k\to(o_k\varphi_k)}(X_{o_k}|X_{\varphi_k})\right]\left[\prod_{k=1}^{n}\Phi^t_{i_k}(X_{i_k}|X_{\partial i_k})\right] \tag{54}$$

or as a marginal of this kind of expressions. The densities Q are defined over the space of all possible configurations of the N-vector $\vec{X}$ of nodes histories.

On the other hand, we may introduce a cavity probability density, q, defined over a reduced space where we partially or completely fix some of the histories. Thus, Q and q are fundamentally different.

Here, we will deal only with cavity probability densities which are defined over connected sets. As in the previous subsection, we can focus on connected sets of the first kind without any loss in generality. The reduction of the configuration space that gives birth to a cavity treatment occurs in this case by fixing the history of one outer node. We can write one of those q densities in terms of local weights and cavity messages from a probability density Q just by removing the cavity messages μ corresponding to the fixed outer node. For example,

$$q^t\left(\vec{X}_{\mathcal{O}\setminus o_j},\vec{X}_{\mathcal{I}}\,||\,X_{o_j}\right) = \left[\prod_{\substack{k=1\\k\neq j}}^{m}\mu^t_{o_k\to(o_k\varphi_k)}\left(X_{o_k}\middle|X_{\varphi_k}\right)\right]\left[\prod_{k=1}^{n}\Phi^t_{i_k}\left(X_{i_k}\middle|X_{\partial i_k}\right)\right]. \tag{55}$$

It is possible to show that the quantities on the left-hand side of (55) can be properly normalized to one, and the relation (55) can be interpreted as an identity only in that case. We will use that interpretation in what follows without loss of generality.

We say that $q^t(\vec{X}_{\mathcal{O}\setminus o_j},\vec{X}_{\mathcal{I}}\,||\,X_{o_j})$ is defined in the cavity where X_{o_j} is fixed, which is represented by the symbol $||$. Figure 3 illustrates this idea by revisiting a particular example shown in the previous subsection.

Let us clarify a bit more the meaning of a cavity relation, in opposition to a conventional conditional relation. Consider a simple stochastic process with two random variables A and B. There, an example of conditional cavity probability density is $p^t(a\,||\,b)$ and the analogous conventional conditional probability density reads $P^t(a|b)$. We have used the notation a and b for some specific values of the variables A and B.

Notice that we used two different symbols to represent conditional and cavity relations: $|$ and $||$, respectively. We remark that these are conceptually different. In this example, the conventional conditional probability density $P^t(a|b)$ is a measure of the set of configurations with $A(t)=a$ restricted to the subspace where $B(t)=b$. However, this magnitude is defined in a stochastic process where A and B can take any of its possible values in the full configuration space. On the other hand, a cavity condition $p^t(a||b)$ is a modification to our stochastic problem whose realizations are now defined on a configuration space where $B(t)=b$ in all cases. If that is not clear, a look back to (55) shows that a cavity density is a result of removing the probabilistic weight that corresponds to the fixed variable (B in this case). The question about what might be happening with B at time t is simply not asked.

With this in mind, we can go on without derivation. By marginalizing (55), we get instantaneous cavity probability densities,

$$p^t\left(\vec{\sigma}_{\mathcal{O}\setminus o_j},\vec{\sigma}_{\mathcal{I}}\,\|\,X_{o_j}\right) = \sum_{\vec{X}_{\mathcal{O}\setminus o_j}|\vec{\sigma}_{\mathcal{O}\setminus o_j}}^{t}\ \sum_{\vec{X}_{\mathcal{I}}|\vec{\sigma}_{\mathcal{I}}}^{t} q^t\left(\vec{X}_{\mathcal{O}\setminus o_j},\vec{X}_{\mathcal{I}}\,\|\,X_{o_j}\right), \tag{56}$$

whose time differentiation is analogous to what we did in the previous subsection. We will have n terms like the ones in the first line of (53) and $m-1$ terms like the ones in the second and third lines of the same equation, only that now everything is defined in the cavity where X_{o_j} is fixed.

Thus, proceeding as in Sec. III B it is easy to verify that

$$\frac{dp^t\left(\vec{\sigma}_{\mathcal{O}\setminus o_j},\vec{\sigma}_{\mathcal{I}}\parallel X_{o_j}\right)}{dt}=-\sum_{l=1}^{n}\left[r_{i_l}(\sigma_{i_l},\sigma_{\partial i_l})\,p^t\left(\vec{\sigma}_{\mathcal{O}\setminus o_j},\vec{\sigma}_{\mathcal{I}}\parallel X_{o_j}\right)-r_{i_l}\left(-\sigma_{i_l},\sigma_{\partial i_l}\right)p^t\left(\vec{\sigma}_{\mathcal{O}\setminus o_j},F_{i_l}[\vec{\sigma}_{\mathcal{I}}]\parallel X_{o_j}\right)\right]$$
$$-\sum_{\substack{l=1\\ l\neq j}}^{m}\sum_{\sigma_{\partial o_l\setminus\varphi_l}}\left[r_{o_l}(\sigma_{o_l},\sigma_{\partial o_l})\,p^t\left(\sigma_{\partial o_l\setminus\varphi_l},\vec{\sigma}_{\mathcal{O}\setminus o_j},\vec{\sigma}_{\mathcal{I}}\parallel X_{o_j}\right)-r_{o_l}(-\sigma_{o_l},\sigma_{\partial o_l})\,p^t\left(\sigma_{\partial o_l\setminus\varphi_l},F_{o_l}\left[\vec{\sigma}_{\mathcal{O}\setminus o_j}\right],\vec{\sigma}_{\mathcal{I}}\parallel X_{o_j}\right)\right]. \tag{57}$$

As (53), Eq. (57) is exact in treelike graphs. However, none of them can be analytically or numerically solved. Equations (53) and (57) contain expressions for the time derivatives of densities $P^t(\vec{\sigma}_{\mathcal{O}},\vec{\sigma}_{\mathcal{I}})$ and $p^t(\vec{\sigma}_{\mathcal{O}\setminus o_j},\vec{\sigma}_{\mathcal{I}}\,||\,X_{o_j})$, but these expressions are not closed on the same variables. They both depend on probability densities defined over bigger sets of nodes.

D. Closure and hierarchical approximations

Although cavity probability densities are defined over configuration spaces which are fundamentally different than the full configuration space of all histories, we can use them to give a closure to equations like (53).

First, let us make a Markovian approximation in Eq. (56) by substituting the full history X_{o_j} by its final state σ_{o_j}:

$$\frac{dp^t\left(\vec{\sigma}_{\mathcal{O}\setminus o_j},\vec{\sigma}_{\mathcal{I}}\parallel \sigma_{o_j}\right)}{dt}=-\sum_{l=1}^{n}\left[r_{i_l}(\sigma_{i_l},\sigma_{\partial i_l})\,p^t\left(\vec{\sigma}_{\mathcal{O}\setminus o_j},\vec{\sigma}_{\mathcal{I}}\parallel \sigma_{o_j}\right)-r_{i_l}\left(-\sigma_{i_l},\sigma_{\partial i_l}\right)p^t\left(\vec{\sigma}_{\mathcal{O}\setminus o_j},F_{i_l}[\vec{\sigma}_{\mathcal{I}}]\big|\sigma_{o_j}\right)\right]$$
$$-\sum_{\substack{l=1\\ l\neq j}}^{m}\sum_{\sigma_{\partial o_l\setminus\varphi_l}}\left[r_{o_l}\left(\sigma_{o_l},\sigma_{\partial o_l}\right)p^t\left(\sigma_{\partial o_l\setminus\varphi_l},\vec{\sigma}_{\mathcal{O}\setminus o_j},\vec{\sigma}_{\mathcal{I}}\parallel \sigma_{o_j}\right)-r_{o_l}\left(-\sigma_{o_l},\sigma_{\partial o_l}\right)p^t\left(\sigma_{\partial o_l\setminus\varphi_l},F_{o_l}\left[\vec{\sigma}_{\mathcal{O}\setminus o_j}\right],\vec{\sigma}_{\mathcal{I}}\parallel \sigma_{o_j}\right)\right]. \tag{58}$$

Equation (58) gives the time derivative of a probability density $p^t(\vec{\sigma}_{\mathcal{O}\setminus o_j},\vec{\sigma}_{\mathcal{I}}\,||\,\sigma_{o_j})$ that can be defined over any connected set in the graph. Its first two lines represent the contribution to the derivative due to flipping rates of spins sitting at inner nodes, and the last two lines correspond to the contribution related to outer nodes (except for σ_{o_j}). As in (53), this equation is not closed. Densities like $p^t(\sigma_{\partial o_l\setminus\varphi_l},\vec{\sigma}_{\mathcal{O}\setminus o_j},\vec{\sigma}_{\mathcal{I}}\,||\,\sigma_{o_j})$ are defined over connected sets which include more nodes than $p^t(\vec{\sigma}_{\mathcal{O}\setminus o_j},\vec{\sigma}_{\mathcal{I}}\,||\,\sigma_{o_j})$. Again, we need closure relations for (58).

1. First-order closures

It is useful at this time to revisit the closure presented in Ref. [5], considered now as the simplest approximation we can make to equations like (58). Indeed, the CME in Ref. [5] is written for the cavity densities $p^t(\sigma_i\,||\,\sigma_j)$, each one involving only two spins. Following (58), the equation for this variables reads

$$\frac{dp^t(\sigma_i\,||\,\sigma_j)}{dt}=-\sum_{\sigma_{\partial i\setminus j}}\{r_i(\sigma_i,\sigma_{\partial i})\,p^t(\sigma_{\partial i\setminus j},\sigma_i\,||\,\sigma_j)-r_i(-\sigma_i,\sigma_{\partial i})\,p^t(\sigma_{\partial i\setminus j},-\sigma_i\,||\,\sigma_j)\}. \tag{59}$$

To close (59), we need to write $p^t(\sigma_{\partial i\setminus j},\sigma_i\,||\,\sigma_j)$ in terms of $p^t(\sigma_i\,||\,\sigma_j)$. To do so in a transparent way, we first make a small detour.

Similarly as in Sec. III C, consider the simple case of a stochastic process with three random variables A, B, and C. There, an example of conditional cavity probability density reads

$$p^t(A=a|B=b\,||\,C=c)=\frac{p^t(a,b\,||\,c)}{p^t(b\,||\,c)}, \tag{60}$$

where a, b, and c are values of the variables A, B, and C. Again, notice that we used two different symbols to represent conditional and cavity relations: | and ||, respectively. Following the language we used in Sec. III C, we say that the density (60) is a measure of the set of configurations with $A(t)=a$ restricted to the subspace where $B(t)=b$ of a stochastic process whose realizations always have $C(t)=c$.

Now, we can write the exact relation:

$$p^t(\sigma_{\partial i\setminus j},\sigma_i\,||\,\sigma_j)=p^t(\sigma_{\partial i\setminus j}|\sigma_i\,||\,\sigma_j)\,p^t(\sigma_i\,||\,\sigma_j). \tag{61}$$

In Ref. [5], this relation is approximated by

$$p^t(\sigma_{\partial i\setminus j}, \sigma_i \,||\, \sigma_j) = p^t(\sigma_{\partial i\setminus j}|\sigma_i \,||\, \sigma_j)\, p^t(\sigma_i \,||\, \sigma_j) \approx \left[\prod_{k\in\partial i\setminus j} p^t(\sigma_k \,||\sigma_i)\right] p^t(\sigma_i \,||\, \sigma_j). \tag{62}$$

The substitution in (62) can be interpreted as a series of changes made to $p^t(\sigma_{\partial i\setminus j}|\sigma_i \,||\, \sigma_j)$. First, the cavity relation with σ_j is dropped to get $p^t(\sigma_{\partial i\setminus j}|\sigma_i \,||\, \sigma_j) \approx p^t(\sigma_{\partial i\setminus j}|\sigma_i)$. Then, the conditional relation with σ_i is substituted by a cavity relation $p^t(\sigma_{\partial i\setminus j}|\sigma_i) \approx p^t(\sigma_{\partial i\setminus j} \,||\, \sigma_i)$. These approximations increase their accuracy when the correlations between $\sigma_{\partial i\setminus j}$, σ_j and σ_i decrease [5].

Completely dropping the dependence on σ_j looks more drastic than replacing $|\sigma_i$ by $\,||\,\sigma_i$, but we must notice that node j is farther apart from any node in $\partial i \setminus j$ than node i, thus, $\sigma_{\partial i\setminus j}$ should be less correlated with σ_j than with σ_i. Finally, it is easy to see that $p^t(\sigma_{\partial i\setminus j} \,||\, \sigma_i)$ can be exactly factorized to get (62), and we obtain the CME as presented in [5]:

$$\frac{dp^t(\sigma_i \,||\, \sigma_j)}{dt} = -\sum_{\sigma_{\partial i\setminus j}} \left\{ r_i(\sigma_i, \sigma_{\partial i}) \left[\prod_{k\in\partial i\setminus j} p^t(\sigma_k \,||\, \sigma_i)\right] p^t(\sigma_i \,||\, \sigma_j) - r_i(-\sigma_i, \sigma_{\partial i}) \left[\prod_{k\in\partial i\setminus j} p^t(\sigma_k \,||\, -\sigma_i)\right] p^t(-\sigma_i \,||\, \sigma_j) \right\}. \tag{63}$$

In Refs. [5–7,13] these kinds of equations are integrated together with

$$\frac{dP^t(\sigma_i)}{dt} = -\sum_{\sigma_{\partial i}} \left\{ r_i(\sigma_i, \sigma_{\partial i}) \left[\prod_{k\in\partial i} p^t(\sigma_k \,||\sigma_i)\right] P^t(\sigma_i) - -r_i(-\sigma_i, \sigma_{\partial i}) \left[\prod_{k\in\partial i} p^t(\sigma_k \,||\, -\sigma_i)\right] P^t(-\sigma_i) \right\}, \tag{64}$$

where a similar factorization is used:

$$P^t(\sigma_{\partial i}, \sigma_i) = P^t(\sigma_{\partial i}|\sigma_i) P^t(\sigma_i) \approx p^t(\sigma_{\partial i} \,||\, \sigma_i)\, P^t(\sigma_i) = \left[\prod_{k\in\partial i} p^t(\sigma_k \,||\sigma_i)\right] P^t(\sigma_i). \tag{65}$$

Although these equations had proven their utility in previous works, we can go beyond Eq. (63) by directly obtaining the time dependence of the probability densities $p^t(\sigma_{\partial i\setminus j}, \sigma_i \,||\, \sigma_j)$. These are defined over a larger connected sets, and according to the general equation (58) its time derivative can be written as

$$\begin{aligned}\frac{dp^t(\sigma_{\partial i\setminus j}, \sigma_i \,||\, \sigma_j)}{dt} &= -r_i(\sigma_i, \sigma_{\partial i})\, p^t(\sigma_{\partial i\setminus j}, \sigma_i \,||\, \sigma_j) + r_i(-\sigma_i, \sigma_{\partial i})\, p^t(\sigma_{\partial i\setminus j}, -\sigma_i \,||\, \sigma_j) \\ &\quad - \sum_{l\in\partial i\setminus j} \sum_{\sigma_{\partial l\setminus i}} \{ r_l(\sigma_l, \sigma_{\partial l})\, p^t(\sigma_{\partial l\setminus i}, \sigma_{\partial i\setminus j}, \sigma_i \,||\, \sigma_j) - r_l(-\sigma_l, \sigma_{\partial l})\, p^t(\sigma_{\partial l\setminus i}, F_l[\sigma_{\partial i\setminus j}], \sigma_i \,||\, \sigma_j) \}. \end{aligned} \tag{66}$$

Again, we need to close these equations introducing some relation between the probability densities $p^t(\sigma_{\partial l\setminus i}, \sigma_{\partial i\setminus j}, \sigma_i \,||\, \sigma_j)$ and $p^t(\sigma_{\partial i\setminus j}, \sigma_i \,||\, \sigma_j)$. We can always concentrate on conditional cavity densities, which allow us to write

$$p^t(\sigma_{\partial l\setminus i}, \sigma_{\partial i\setminus j}, \sigma_i \,||\, \sigma_j) = p^t(\sigma_{\partial l\setminus i}|\sigma_{\partial i\setminus j}, \sigma_i \,||\, \sigma_j)\, p^t(\sigma_{\partial i\setminus j}, \sigma_i \,||\, \sigma_j). \tag{67}$$

As before, we can take $p^t(\sigma_{\partial l\setminus i}|\sigma_{\partial i\setminus j}, \sigma_i \,||\, \sigma_j)$ and drop the dependence on σ_j. As all nodes in $\partial i \setminus j$, except for l, are at the same distance from any node in $\partial l \setminus i$ than node j, the corresponding spins will be in average equally correlated with $\sigma_{\partial l\setminus i}$ than σ_j. Let us also drop the conventional conditional dependence on these nodes to get the relation $p^t(\sigma_{\partial l\setminus i}|\sigma_{\partial i\setminus j}, \sigma_i \,||\, \sigma_j) \approx p^t(\sigma_{\partial l\setminus i}|\sigma_l, \sigma_i)$. This procedure is now more accurate than with (63), because we are neglecting correlations associated with nodes which are farther apart in the graph.

Then, we replace the conventional conditional relation with σ_i by a cavity relation to obtain

$$p^t(\sigma_{\partial l\setminus i}|\sigma_{\partial i\setminus j}, \sigma_i \,||\, \sigma_j) \approx p^t(\sigma_{\partial l\setminus i}|\sigma_l \,||\, \sigma_i) = \frac{p^t(\sigma_{\partial l\setminus i}, \sigma_l \,||\, \sigma_i)}{\sum_{\sigma_{\partial l\setminus i}} p^t(\sigma_{\partial l\setminus i}, \sigma_l \,||\, \sigma_i)}. \tag{68}$$

With this, we have closed (66) through approximations for conditional cavity probability densities.

Equations (66) and (68) must also be combined with differential equations for the probability densities P^t. In this case, we can use, for example,:

$$\begin{aligned}\frac{dP^t(\sigma_{\partial i}, \sigma_i)}{dt} &= -r_i(\sigma_i, \sigma_{\partial i})\, P^t(\sigma_{\partial i}, \sigma_i) + r_i(-\sigma_i, \sigma_{\partial i})\, P^t(\sigma_{\partial i}, -\sigma_i) \\ &\quad - \sum_{l\in\partial i} \sum_{\sigma_{\partial l\setminus i}} \{ r_l(\sigma_l, \sigma_{\partial l})\, p^t(\sigma_{\partial l\setminus i}|\sigma_l \,||\, \sigma_i)\, P^t(\sigma_{\partial i}, \sigma_i) - r_l(-\sigma_l, \sigma_{\partial l})\, p^t(\sigma_{\partial l\setminus i}| - \sigma_l \,||\, \sigma_i)\, P^t(F_l[\sigma_{\partial i}], \sigma_i) \}, \end{aligned} \tag{69}$$

which involves essentially the same approximations than (69):

$$P^t(\sigma_{\partial l\setminus i}, \sigma_{\partial i}, \sigma_i) = P^t(\sigma_{\partial l\setminus i}|\sigma_{\partial i}, \sigma_i)\, P^t(\sigma_{\partial i}, \sigma_i) \approx p^t(\sigma_{\partial l\setminus i}|\sigma_l \,||\sigma_i\,)\, P^t(\sigma_{\partial i}, \sigma_i). \tag{70}$$

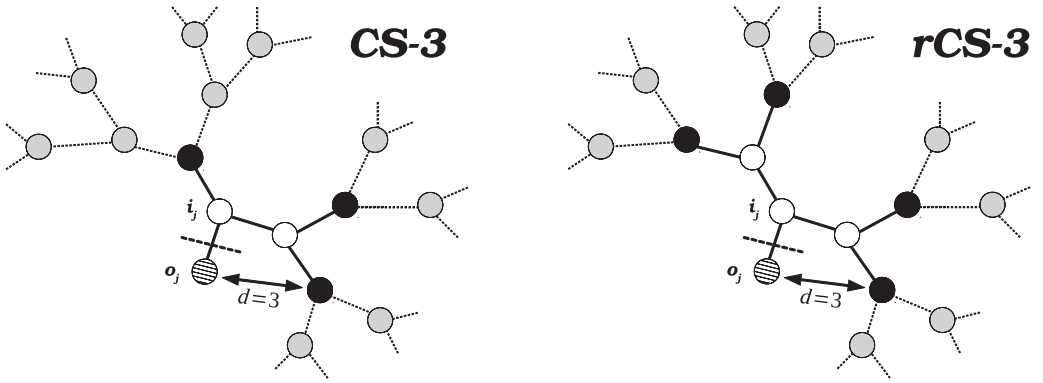

(a) (b)

FIG. 4. A cavity probability density $p^t(\vec{\sigma}_{\mathcal{O}\setminus o_j}, \vec{\sigma}_{\mathcal{I}} \,||\, \sigma_{o_j})$ is defined over a general connected set. This figure illustrates the classification of these sets according to the distance between the outer nodes and the origin o_j. (a) The maximum distance is $d = 3$. Thus, the set belongs to class *CS-3*. In this example, all distances are not equal. (b) Every outer node is at a distance $d = 3$ from o_j. Thus, the set is *rCS-3* and belongs to *CS-3*.

The performance of the set of equations (66)–(70) that we call in the following CME-2 will outperform the CME as presented in Ref. [5] [see Eqs. (63) and (64)]. This is illustrated below in Sec. IV.

2. General closure

Although we gave an initial idea of how to use the dynamic cavity method to obtain closed systems of differential equations for local probability densities, our goal is to provide a general method that works for any equation like (57). This requires some sense of structure and order that should facilitate the reader's comprehension. We will move among connected sets of the first kind (see Fig. 1) to establish a hierarchy using the concept of distance within the graph.

We can find a path that connects every pair of nodes in a connected set. Furthermore, for each pair there is always a path with minimum length, and we can define a distance between nodes as the length of that minimal path. The distance $d(k, l)$ between nodes k and l, with $k \neq l$, is then a positive integer.

From this, we can classify the connected set $\{\mathcal{O} \setminus o_j, \mathcal{I}, o_j\}$ according to the distances between the node o_j (the origin) and all the outer nodes $\mathcal{O} \setminus o_j$. When the maximum distance $\max_{o_l \in \mathcal{O}\setminus o_j}\{d(o_j, o_l)\}$ is equal to the integer Z, we will say that the connected set is in the class *CS-Z*. If all the outer nodes (except o_j) are at the same distance from o_j,i.e., if $d(o_j, o_l) = d(o_j, o_k)$ for all $o_k, o_l \in \mathcal{O} \setminus o_j$, we will say that the connected set is regular and use the notation *rCS-Z* to refer to that specific set. Of course, every *rCS-Z* belongs to the class *CS-Z*. Figure 4 illustrates this classification.

In this context, we can use the notation

$$p^t\left(\vec{\sigma}_{\mathcal{O}\setminus o_j}, \vec{\sigma}_{\mathcal{I}} \,\|\, \sigma_{o_j}\right) \equiv p^t\left(\vec{\sigma}_Z, \vec{\sigma}_{Z-1}, \ldots, \vec{\sigma}_2, \vec{\sigma}_1 \,\|\, \sigma_{o_j}\right) \equiv p^t\left(\vec{\sigma}_Z, \vec{\sigma}_{Z-1}, \ldots, \vec{\sigma}_2, \sigma_{i_j} \,\|\, \sigma_{o_j}\right), \tag{71}$$

where i_j is the inner node connected to o_j.

In (71), the vector $\vec{\sigma}_z$ $(1 \leqslant z \leqslant Z)$ contains the spins σ_k such that $d(k, o_j) = z$, with the condition that $k \in \mathcal{O}$ or $k \in \mathcal{I}$. The cavity probability density in (71) is defined over a connected set that belongs to the class *CS-Z*, which we will represent with the symbol $p^t(CS\text{-}Z)$. To simplify our language, we will simply say that all $p^t(CS\text{-}Z)$ are *in CS-Z*.

Using our new notation (71), the cavity probability densities in the last two lines of (58), which are in *CS-(*Z + 1*)*, can be rewritten as

$$p^t\left(\sigma_{\partial o_l\setminus\varphi_l}, \vec{\sigma}_{\mathcal{O}\setminus o_j}, \vec{\sigma}_{\mathcal{I}} \,\middle|\, \sigma_{o_j}\right) \equiv p^t\left(\vec{\sigma}_{Z+1}, \vec{\sigma}_Z, \vec{\sigma}_{Z-1}, \ldots, \vec{\sigma}_2, \sigma_{i_j} \,\|\, \sigma_{o_j}\right), \tag{72}$$

where $\vec{\sigma}_{Z+1}$ is exactly the same than $\sigma_{\partial o_l\setminus\varphi_l}$.

Notice that every $p^t(CS\text{-}Z)$ is a marginal of a cavity probability density defined over the corresponding regular set *rCS-Z* (see left panels of Fig. 4). In view of all this, what we need to write is a system of equations like

$$\frac{dp^t(rCS\text{-}Z)}{dt} = F[p^t(rCS\text{-}Z)], \tag{73}$$

which in our case is equivalent to find a relation $p^t(CS\text{-}(Z{+}1)) = f[p^t(CS\text{-}Z)]$.

With this classification of connected sets according, essentially, to their size, we are ready to find that $f[\cdot]$ function. Let us write

$$p^t\left(\vec{\sigma}_{Z+1}\middle|\vec{\sigma}_Z, \ldots, \sigma_{i_j} \,\|\, \sigma_{o_j}\right) = \frac{p^t\left(\vec{\sigma}_{Z+1}, \vec{\sigma}_Z, \ldots, \sigma_{i_j} \,\|\, \sigma_{o_j}\right)}{p^t\left(\vec{\sigma}_Z, \ldots, \sigma_{i_j} \,\|\, \sigma_{o_j}\right)}. \tag{74}$$

If the distance $Z+1$ is large compared to the system's correlation length, we can assume that the fact of having fixed the value of σ_{o_j} at time t is irrelevant for the state $\vec{\sigma}_{Z+1}$ on the left-hand side of (73):

$$p^t\left(\vec{\sigma}_{Z+1}\middle|\vec{\sigma}_Z,\ldots,\sigma_{i_j}\parallel\sigma_{o_j}\right)\approx p^t\left(\vec{\sigma}_{Z+1}|\vec{\sigma}_Z,\ldots,\vec{\sigma}_2,\sigma_{i_j}\right). \tag{75}$$

Following the same reasoning, we can drop all the spins in $\{\vec{\sigma}_Z,\ldots,\vec{\sigma}_2\}$ whose distance to the nodes in $\vec{\sigma}_{Z+1}$ is larger than Z. We have already done this kind of approximation when writing the equations for $p^t(\sigma_i\,||\sigma_j)$ and $p^t(\sigma_{\partial i\setminus j},\sigma_i\,||\sigma_j)$; here we are just generalizing. The remaining spins $\{\vec{\sigma}_{Z+1},\vec{\sigma}'_Z,\ldots,\vec{\sigma}'_2,\sigma_{i_j}\}$ are defined over a connected set of the class *CS-Z*, with origin in i_j.

Furthermore, when the spatial correlation between $\vec{\sigma}_{Z+1}$ and σ_{i_j} is low, we can make the approximation [5]

$$p^t\left(\vec{\sigma}_{Z+1}|\vec{\sigma}'_Z,\ldots,\vec{\sigma}'_2,\sigma_{i_j}\right)\approx p^t\left(\vec{\sigma}_{Z+1}|\vec{\sigma}'_Z,\ldots,\vec{\sigma}'_2\parallel\sigma_{i_j}\right)=\frac{p^t\left(\vec{\sigma}_{Z+1},\vec{\sigma}'_Z,\ldots,\vec{\sigma}'_2\parallel\sigma_{i_j}\right)}{p^t\left(\vec{\sigma}'_Z,\ldots,\vec{\sigma}'_2\parallel\sigma_{i_j}\right)}. \tag{76}$$

Notice that the distance between i_j and the nodes related to $\vec{\sigma}_{Z+1}$ is equal to Z, so we are assuming that the correlation decays noticeably at that distance.

From (75) and (76), we have

$$p^t\left(\vec{\sigma}_{Z+1}|\vec{\sigma}_Z,\ldots,\sigma_{i_j}\parallel\sigma_{o_j}\right)\approx\frac{p^t\left(\vec{\sigma}_{Z+1},\vec{\sigma}'_Z,\ldots,\vec{\sigma}'_2\mid\sigma_{i_j}\right)}{\sum_{\vec{\sigma}_{Z+1}}p^t\left(\vec{\sigma}_{Z+1},\vec{\sigma}'_Z,\ldots,\vec{\sigma}'_2\parallel\sigma_{i_j}\right)}, \tag{77}$$

and the probability densities (72) become

$$\begin{aligned}p^t\left(\vec{\sigma}_{Z+1},\vec{\sigma}_Z,\ldots,\sigma_{i_j}\mid\sigma_{o_j}\right)&=p^t\left(\vec{\sigma}_{Z+1}|\vec{\sigma}_Z,\ldots,\sigma_{i_j}\mid\sigma_{o_j}\right)p^t\left(\vec{\sigma}_Z,\ldots,\sigma_{i_j}\parallel\sigma_{o_j}\right),\\ p^t\left(\vec{\sigma}_{Z+1},\vec{\sigma}_Z,\ldots,\sigma_{i_j}\parallel\sigma_{o_j}\right)&\approx\frac{p^t\left(\vec{\sigma}_{Z+1},\vec{\sigma}'_Z,\ldots,\vec{\sigma}'_2\mid\sigma_{i_j}\right)}{\sum_{\vec{\sigma}_{Z+1}}p^t\left(\vec{\sigma}_{Z+1},\vec{\sigma}'_Z,\ldots,\vec{\sigma}'_2\parallel\sigma_{i_j}\right)}p^t\left(\vec{\sigma}_Z,\ldots,\sigma_{i_j}\parallel\sigma_{o_j}\right).\end{aligned} \tag{78}$$

Thus, we have managed to write the function $f[p^t(CS\text{-}Z)]$ that gives any cavity probability density in *CS-(Z + 1)* in terms of several densities in *CS-Z*. This constitutes a closure for (58), and we can now numerically solve these equations.

It is important to say that after solving for $p^t(CS\text{-}Z)$, we can compute all the cavity probability densities in *CS-1*, *CS-2*,..., *CS-(Z-1)* as its marginals.

As for (53), we can write $P^t(\sigma_{\partial o_l\setminus\varphi_l},\vec{\sigma}_{\mathcal{O}},\vec{\sigma}_{\mathcal{I}})$ in terms of $P^t(\vec{\sigma}_{\mathcal{O}},\vec{\sigma}_{\mathcal{I}})$ and a cavity probability density whose value we can obtain from the numerical integration of (58) with the relation (78). We do

$$\begin{aligned}P^t\left(\sigma_{\partial o_l\setminus\varphi_l},\vec{\sigma}_{\mathcal{O}},\vec{\sigma}_{\mathcal{I}}\right)&=P^t\left(\sigma_{\partial o_l\setminus\varphi_l}\middle|\vec{\sigma}_{\mathcal{O}},\vec{\sigma}_{\mathcal{I}}\right)P^t(\vec{\sigma}_{\mathcal{O}},\vec{\sigma}_{\mathcal{I}}),\\ P^t\left(\sigma_{\partial o_l\setminus\varphi_l},\vec{\sigma}_{\mathcal{O}},\vec{\sigma}_{\mathcal{I}}\right)&\approx p^t\left(\sigma_{\partial o_l\setminus\varphi_l}|\vec{\sigma}_{\mathcal{O}\setminus o_j},\vec{\sigma}_{\mathcal{I}}\,\middle|\sigma_{o_j}\right)P^t(\vec{\sigma}_{\mathcal{O}},\vec{\sigma}_{\mathcal{I}}).\end{aligned} \tag{79}$$

Here we changed the conditional probability density $P^t(\sigma_{\partial o_l\setminus\varphi_l}|\vec{\sigma}_{\mathcal{O}},\vec{\sigma}_{\mathcal{I}})$ by a conditional cavity density. Nevertheless, we introduced the cavity condition by fixing only the spin σ_{o_j}. Again, this substitution should be accurate when the distance between o_j and the nodes in $\partial o_l\setminus\varphi_l$ is large enough compared with correlation length. Finally, Eqs. (58), (74), (78), and (79) give a closure to the differential Eq. (53) and we are ready to numerically obtain the time dependence of system's observables.

It is important to say that our closure relations could be used in several ways, but the key point will always be how to choose the distance Z at which we neglect correlations and substitute conventional conditional relations by conditional cavity relations. This distance will be the parameter that defines what we will call a *level of approximation*.

Summarizing, we define a level of approximation through the differential equations for the cavity probability densities (58). If we write them for densities $p^t(CS\text{-}Z)$, we say that we are in the Zth level of approximation. Within this context, Eqs. (63) and (64) constitute a first-level approximation and we will say they are *in* the level CME-1. On the other hand, Eqs. (66)–(70) are *in* the second level, which is CME-2.

IV. NUMERICAL RESULTS

The information about the nature of the interactions and the local dynamics goes into the spin-flip rates $r_i(\sigma_i,\sigma_{\partial i})$, which of course depend on the graph's structure. Here, we will work over two families of diluted random graphs which are locally treelike: Erdos-Renyi [24] and random regular graphs.

In practice, once interactions are set, we select an initial condition for all probability densities (P^{t_0} and p^{t_0}), and the integration of the equations gives the full P^t and p^t. In Sec. IV A, we will explore the numerical differences obtained with first and second levels of approximation, CME-1 and CME-2, into two well-known spin models from statistical mechanics, the Ising ferromagnet and the Viana-Bray spin-glass, both defined over Erdos-Renyi graphs. In Sec. IV B, we compare CME-2 and CME-3 with the dynamical independent neighbor approximation (DINA) presented in Ref. [22] for the dynamics of the Ising ferromagnet. Finally, in Sec. IV C we also contrast the results of CME-2, with the ones of pair quenched mean-field approximation for the dynamics of the SIS model for epidemics [25,26].

A. First and second levels of approximation

One of the traditional forms that theorists choose for the spin flipping probabilities per time unit is Glauber's

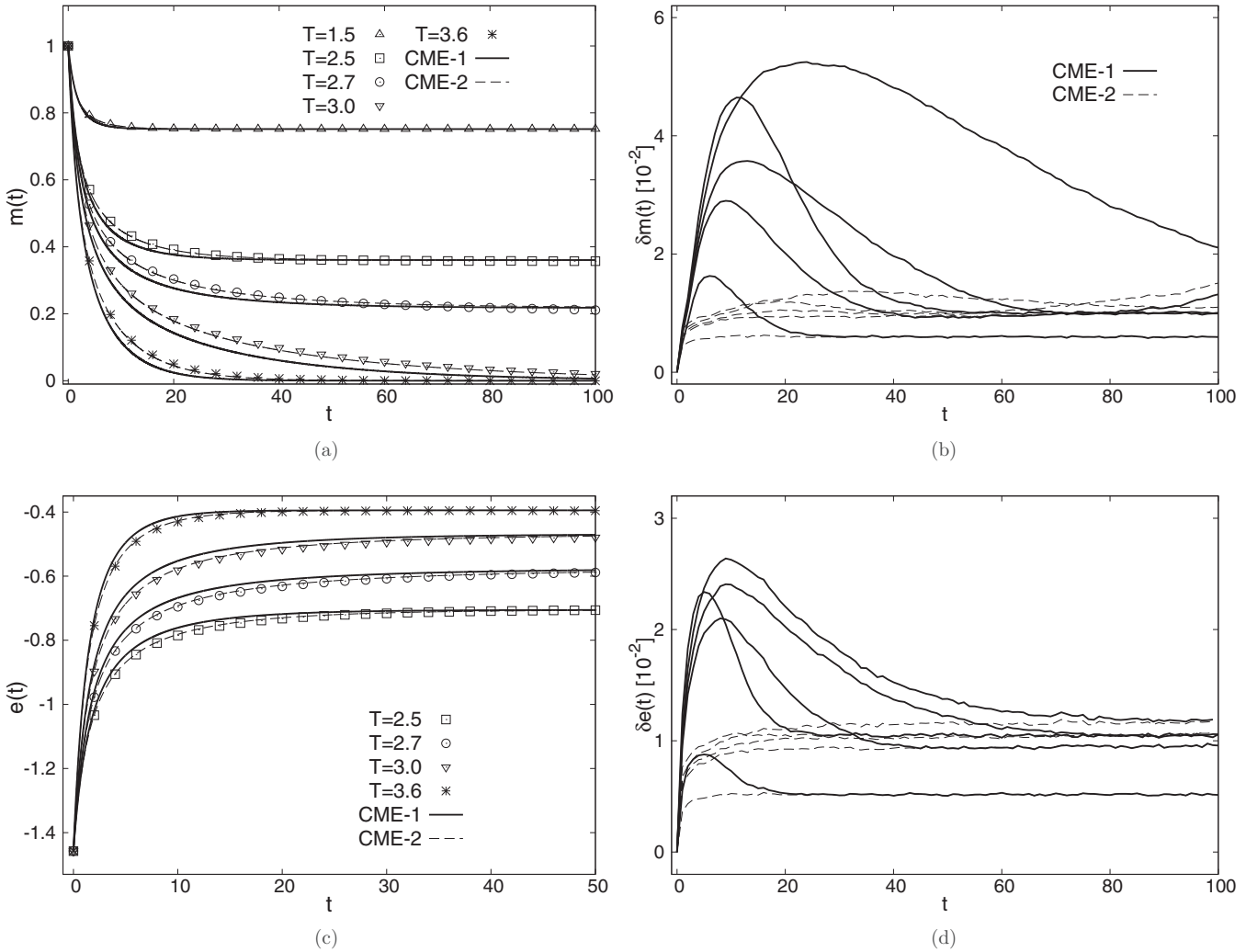

FIG. 5. Dynamics of the Ising ferromagnet according to kinetic Monte Carlo simulations (points), and the integration of equations in levels CME-1 (thick lines) and CME-2 (dashed lines). In all cases, an initially fully magnetized system evolves in time in contact with a heat bath at a given temperature. Calculations were done for Erdos-Renyi graphs of size $N = 5000$ with mean connectivity $c = 3$. (a) Time evolution of system's magnetization [see Eq. (83)]. (b) Time evolution of the error (84) between local magnetizations predicted by CME-1, 2, and the results of kinetic Monte Carlo simulations. (c) Time evolution of system's energy density [see Eq. (85)]. (d) Time evolution of the error (86) written for the expected values of local energy terms.

rule [8]:

$$r_i(\sigma_i, \sigma_{\partial i}) = \frac{1}{2}\left[1 - \sigma_i \tanh\left(\beta \sum_{k\in\partial i} J_{ki}\sigma_k + \beta h_i\right)\right]. \quad (80)$$

As usual, the spin variables σ_i can take the values $\sigma_i = \pm 1$. The interaction between each pair of connected spins (σ_i, σ_j) is encoded in the couplings parameters $J_{ij} = \pm 1$ and can be either satisfied ($J_{ij}\sigma_i\sigma_j = 1$) or unsatisfied ($J_{ij}\sigma_i\sigma_j = -1$). On the other hand, the h_i are local fields that we will set here to zero. The parameter β is the inverse of the temperature T.

We can then write

$$r_i(\sigma_i, \sigma_{\partial i}) \equiv r_i(c_i, u_i) = \tfrac{1}{2}[1 - \tanh(\beta(c_i - 2u_i))], \quad (81)$$

where c_i is spin's connectivity and we can use the Kronecker's delta to write

$$u_i \equiv u_i(\sigma_i, \sigma_{\partial i}) = \sum_{k\in\partial i} \delta_{J_{ki}, -\sigma_k\sigma_i}. \quad (82)$$

When the number u_i of unsatisfied interactions between i and its neighbors is large, there is a high probability that σ_i changes to $-\sigma_i$ [see Eq. (81)].

Let us assume we have an Erdos-Renyi graph with N nodes, and in every node a spin variable. The corresponding ferromagnetic Ising model is the result of setting $J_{ij} = 1$ for all the connected pairs (i, j). With this definition and with the rules (81) we can make kinetic Monte Carlo simulations of the system's dynamics.

Figure 5 shows results of these simulations alongside the semianalytical output of our dynamic cavity method in the first (CME-1) and second (CME-2) levels of approximation. These results were obtained by integrating Eqs. (63), (64), and (66)–(70), respectively. In all cases, the initial condition is a configuration with all spins pointing up. Top-left panel contains the time evolution of the system's magnetization [Eq. (83)], while top-right panel illustrates the corresponding error for the local magnetization [Eq. (84)] between a

theoretical approach and the simulation (MC):

$$m(t) = \frac{1}{N}\sum_{i=1}^{N}\sum_{\sigma_i}\sigma_i P^t(\sigma_i) \equiv \frac{1}{N}\sum_{i=1}^{N} m_i(t), \tag{83}$$

$$\delta m^{\mathrm{TH}}(t) = \sqrt{\frac{1}{N}\sum_{i=1}^{N}\left(m_i^{\mathrm{TH}}(t) - m_i^{\mathrm{MC}}(t)\right)^2}, \tag{84}$$

The behavior depicted in the top-left panel is typical of ferromagnets. A transition between two regimes occurs at some $T_C = (\mathrm{arctanh}[1/c])^{-1}$ [27] (when the average connectivity is $c = 3$, we have $T_C \approx 2.89$). In the thermodynamic limit, the spin's up-down symmetry is broken, steady-state magnetization is zero for high temperatures ($T > T_C$), and at low temperatures ($T < T_C$) we have nonzero magnetization for all times.

Both levels of approximation, CME-1 and CME-2, give a good qualitative and quantitative description of the magnetization obtained from the simulations, especially at the steady state. This is not surprising. In the cases where the steady state is governed by a Boltzmann distribution, the long-time limit of our dynamical scheme is equivalent to the traditional equilibrium cavity method [13]. This means that on the ferromagnet we will get the well-known belief propagation (BP) solutions by integrating our dynamical equations for long enough. At treelike networks, which here implies taking the thermodynamic limit, the fixed point of BP is the exact solution of the problem. Finite-size effects are responsible for the discrepancies between the steady state of our equations and the simulations.

The results of CME-2 are particularly accurate, in the steady state and in the transient. The top-right panel of Fig. 5 shows CME-2 reproduces local magnetizations $m_i^{\mathrm{MC}}(t)$ also quite well, with errors of order $10^{-3} - 10^{-2}$.

The bottom-left panel of Fig. 5 shows the time evolution of the ferromagnet's energy density,

$$e(t) = -\frac{1}{2N}\sum_{i\neq j}\sum_{\sigma_i}\sum_{\sigma_j} P^t(\sigma_i,\sigma_j) J_{ij}\sigma_i\sigma_j = \frac{1}{2}\sum_{i\neq j} e_{ij}(t), \tag{85}$$

which is a measure of how many unsatisfied interactions are in the system. Again, our dynamic cavity method gives very accurate results, even for the expected values of local energy terms $e_{ij}(t)$. The bottom-right panel of Fig. 5 shows the time evolution of the local error,

$$\delta e^{\mathrm{TH}}(t) = \sqrt{\frac{1}{2M}\sum_{i\neq j}\left(e_{ij}^{\mathrm{TH}}(t) - e_{ij}^{\mathrm{MC}}(t)\right)^2}, \tag{86}$$

where M is the number of connected pairs (i, j). This error remains of order $10^{-3} - 10^{-2}$ for all times.

Another way of choosing the couplings is to draw each one from the bimodal distribution $d(J_{ij}) = 1/2\delta(J_{ij} - 1) + 1/2\delta(J_{ij} + 1)$. In this model, also defined over Erdos-Renyi random graphs, we have a transition to a spin-glass phase at a finite temperature T_{SG}. As correlations play an important role when temperature decreases, we know that the approximations we made in Sec. III D cannot be as accurate as with the ferromagnet.

Figure 6 shows results for this model in a graph with $c = 3$, where the transition temperature is $T_{\mathrm{SG}} = (\mathrm{arctanh}[\sqrt{1/c}])^{-1} \approx 1.52$ [28]. As expected, below T_{SG} the description is not as successful as for the ferromagnetic case. However, it still holds that CME-2 performs better than CME-1. In the top-right panel, we see that for $0 \leqslant t \leqslant 100$ the errors are on a scale of 10^{-1}, which is one order higher than what we saw in the ferromagnet. Furthermore, even with the approximation CME-2, the error seems to monotonically increase with time.

However, our theoretical description of the simulations is noticeably improved just by going up one level in our hierarchical approximations. Not only errors for local magnetizations are appreciably smaller with level CME-2 than with CME-1. If we look at the bottom panels of the figure, we see how this second level of approximation already gives a good description of the average $e(t)$ even at very low temperatures like $T = 0.25 \ll T_{\mathrm{SG}}$. However, this result might be misleading because the errors for the expected values of local energy terms are still of order 10^{-1}.

Results in Figs. 5 and 6 indicate that the performance of the approach used in Refs. [5–7,13] (in CME-1) is significantly improved just by using the next level of approximation. It is important to say that the integration of equations in the second level, although very accurate, does not take high effort, considering the capabilities of present-day personal computers, not to mention high-performance computers.

B. Comparison with other theoretical approaches

The hierarchical system of approximations introduced for the study of stochastic local search algorithms [20,21] and systematized in Ref. [22] combines theoretical simplicity with numerical accuracy in a variety of traditional models from statistical mechanics. Here, we will compare our theoretical approach with the DINA, which constitutes the second level of the scheme presented in Ref. [22].

In the case of an Ising ferromagnet with Glauber rates (81) defined over random regular graphs, where every node has K neighbors, the DINA works with the exact equation:

$$\begin{aligned}\frac{d\hat{P}^t(\sigma,u)}{dt} &= -r(K,u)\,\hat{P}^t(\sigma,u) + r(K,K-u)\,\hat{P}^t(-\sigma,K-u)\\ &\quad -\sum_{u'=0}^{K-1}(K-u')\,r(K,u')\,\hat{P}^t(\sigma,u')[\hat{P}^t(u|\sigma,\sigma,u') - \hat{P}^t(u-1|\sigma,\sigma,u')]\\ &\quad -\sum_{u'=0}^{K-1}(u'+1)\,r(K,u'+1)\,\hat{P}^t(\sigma,u'+1)[\hat{P}^t(u-1|\sigma,-\sigma,u') - \hat{P}^t(u|\sigma,-\sigma,u')],\end{aligned} \tag{87}$$

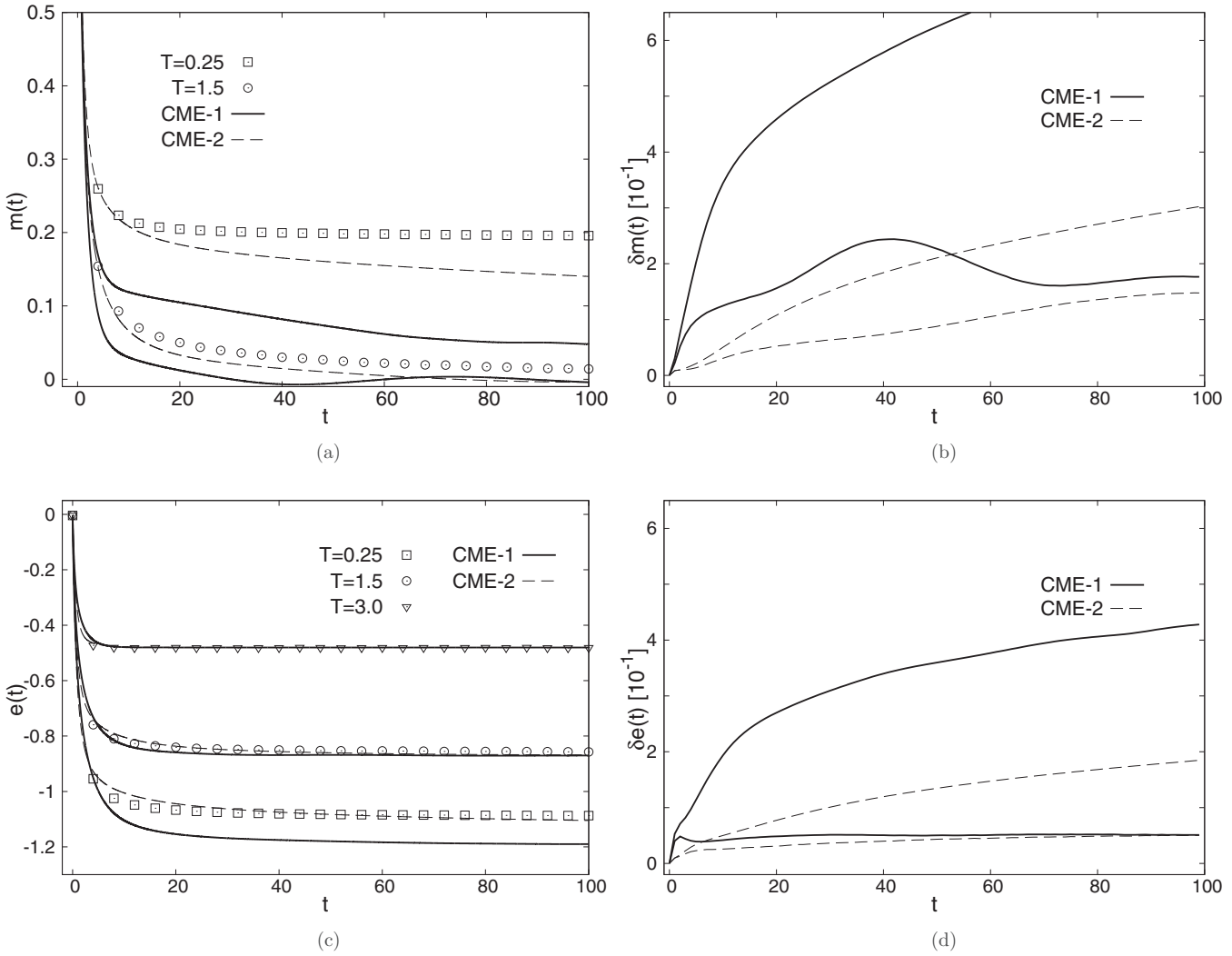

FIG. 6. Dynamics of the Viana-Bray spin glass according to kinetic Monte Carlo simulations (points), and the integration of equations in levels CME-1 (thick lines) and CME-2 (dashed lines). In all cases, an initially fully magnetized system evolves in time in contact with a heat bath at a given temperature. Calculations were done for Erdos-Renyi graphs of size $N = 1000$ with mean connectivity $c = 3$. (a) Time evolution of system's magnetization [see Eq. (83)]. (b) Time evolution of the error (84) between local magnetizations predicted by CME-1, 2, and the results of kinetic Monte Carlo simulations. (c) Time evolution of system's energy density [see Eq. (85)]. (d) Time evolution of the error (86) written for the expected values of local energy terms.

together with the closure relations [22]:

$$\hat{P}^t(\hat{u}|\sigma,\sigma,\hat{u}') \approx \frac{(K-\hat{u})\hat{P}^t(\sigma,\hat{u})}{\sum_{u'}(K-u')\,\hat{P}^t(\sigma,u')}, \tag{88}$$

$$\hat{P}^t(\hat{u}|\sigma,-\sigma,\hat{u}') \approx \frac{(\hat{u}+1)\hat{P}^t(\sigma,\hat{u}+1)}{\sum_{u'}u'\,\hat{P}^t(\sigma,u')}. \tag{89}$$

Here, $r(K,u) \equiv r_i(c_i = K, u_i = u)$ [see Eq. (81)] and $\hat{P}^t(\sigma,u)$ is the probability density of having a node with spin σ and u unsatisfied interactions with its neighbors. The variable u is an integer between zero and K. This can be written in terms of the densities $P^t(\sigma_i,\sigma_{\partial i})$ as

$$\hat{P}^t(\sigma,u) = \lim_{N\to\infty} \ll \frac{1}{N}\sum_{i=1}^{N}\sum_{\sigma_i}\sum_{\sigma_{\partial i}} P^t_{\xi_K(N)}(\sigma_i,\sigma_{\partial i})\,\delta_{\sigma,\sigma_i} \times \delta_{(\sum_{k\in\partial i}\sigma_k),K-2u} \gg_{\xi_K(N)}, \tag{90}$$

where $\xi_K(N)$ is the ensemble of random regular graphs with connectivity K and size N, and $\delta_{x,y}$ is a Kronecker delta evaluated at (x,y). The symbol $\ll\cdot\gg_{\xi_K(N)}$ represents an average over this ensemble, with proper probabilistic weights.

We can similarly define the probability density $\hat{P}^t(\sigma,\sigma',\hat{u},\hat{u}')$ of having a connected pair (σ,σ') with $\hat{u}$ and $\hat{u}'$ unsatisfied interactions with their other neighbors, respectively. In this case, $\hat{u},\hat{u}'$ are integers between zero and $K-1$. The magnitude $\hat{P}^t(\hat{u}|\sigma,\sigma',\hat{u}')$ that we have in (87) is the conditional probability density:

$$\hat{P}^t(\hat{u}|\sigma,\sigma',\hat{u}') = \frac{\hat{P}^t(\sigma,\sigma',\hat{u},\hat{u}')}{\sum_{\hat{u}}\hat{P}^t(\sigma,\sigma',\hat{u},\hat{u}')}. \tag{91}$$

The closure relation used in DINA can be derived starting from the assumptions of the dynamical replica approach under a replica symmetry ansatz [22]. This explains why DINA

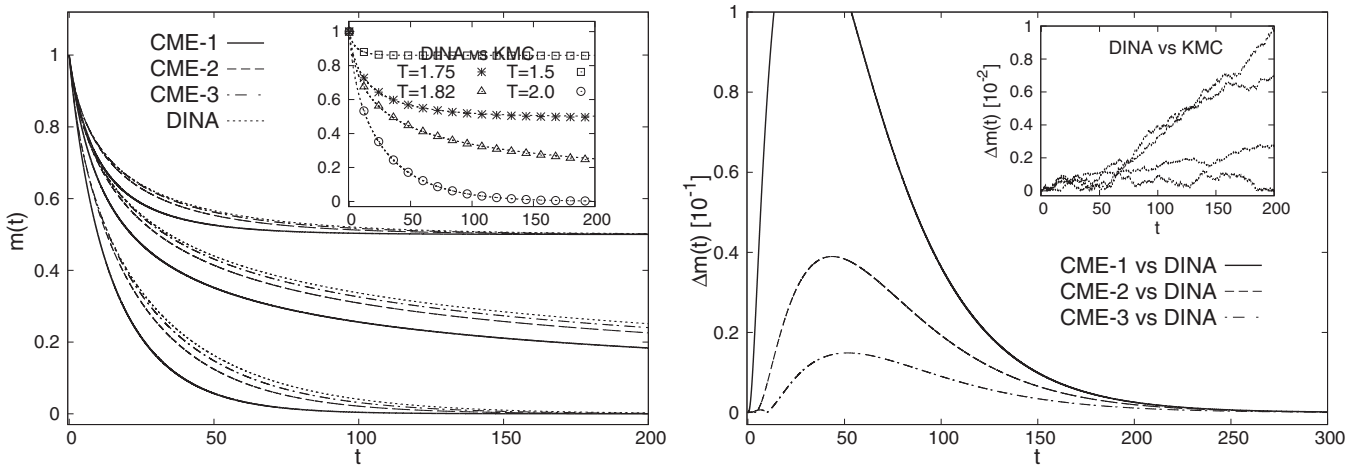

FIG. 7. Comparison between the dynamics of the Ising ferromagnet defined at random regular graphs according to kinetic Monte Carlo simulations (points), the integration of the DINA (thin-dashed lines), and equations in the levels CME-1 (thick lines), CME-2 (dashed lines), and CME-3 (dashed-dotted lines). In all cases, an initially fully magnetized system with mean connectivity $K = 3$ evolves in time in contact with a heat bath at a given temperature. KMC calculations were done for a random regular graph of size $N = 10000$. (a) The main and the inserted graphics show the time evolution of system's magnetization [see Eq. (83)]. The first one compares the different levels of approximation of our dynamic cavity method with the DINA and displays results for $T = 1.75, 1.82, 2.0$ (from top to bottom). The latter compares the DINA with the results of kinetic Monte Carlo simulations and displays results for $T = 1.5, 1.75, 1.82, 2.0$ (from top to bottom). (b) The main graphic shows the absolute difference Δm between the average magnetizations predicted by the DINA and by different levels of approximation of the dynamic cavity method. All curves correspond to $T = 2.0$. The inserted graphic compares the DINA with kinetic Monte Carlo using the same Δm parameter, whose behavior is displayed for $T = 1.82, 1.75, 1.5, 2.0$ (from top to bottom).

gives very accurate results in models where detailed balance holds. In this case, it is more likely that the microscopic probability distribution function is a constant within a subspace with a finite number of order parameters. Indeed, we know that in those models the condition is satisfied at least at equilibrium.

The inserted plot on the left panel of Fig. 7 shows very good agreement between the average magnetizations predicted by the DINA and the KMC simulations for the Ising ferromagnet defined over random regular graphs. This is complemented by the inserted plot on the right panel. It is important to notice that the DINA is not written for single instances and, therefore, it cannot give local information. This means that Eq. (84) is not applicable here and we need to define a new *error*. The simplest one is the absolute difference between the average magnetizations, a parameter that we call Δm (in contrast to δm).

In the inserted plot of the right panel of Fig. 7, Δm is of order 10^{-3} for all times. This speaks very well of the DINA's accuracy when predicting the behavior of the average magnetization, even at finite size systems (in this case $N = 10\,000$).

We already said in Sec. IV A that in the thermodynamic limit, our dynamical cavity method gives the correct solution for the equilibrium of the ferromagnet in random graphs, where it is equivalent to the equilibrium cavity method [13]. Coolen *et al.* established the convergence of DRT under replica symmetry to the standard equilibrium replica symmetric solution [14]. Therefore, the steady state of the DINA and our equations must be equivalent under the conditions described above.

As can be seen, (87) is an average over the graph ensemble of the differential equation for $P^t(\sigma_i, \sigma_{\partial i})$, which has the form (53). Therefore, closure relations (88) and (89) are equivalent to our closure relation (70) in the sense that both are approximations for the same kind of conditional probabilities. Actually, they both drop the information about the number of unsatisfied relations $\hat{u}'$. An important difference is in the fact that the first ones are written for the average case probability densities, while the latter is written for the single instance.

However, for our dynamic cavity method, all sites become equivalent at random regular graphs with homogeneous initial conditions. In that case, all probability densities defined over connected sets with the same structure follow the same differential equations. We can drop information about the local structure of the graph. As we show in Appendix C, we can forget the irrelevant details of, let us say, $P^t(\sigma_i, \sigma_{\partial i})$. All the combinations of σ_i, $\sigma_{\partial i}$ with the same value of σ_i and the same number of unsatisfied interactions between this spin and its neighborhood will have the same probability density $P^t(\sigma = \sigma_i, u = \sum_{k\in\partial i} \delta_{\sigma_k,-\sigma_i})$.

We are easily able to write average case equations (see Appendix C) for several levels of approximation, as the density (90) can be directly written as $\hat{P}^t(\sigma, u) = \binom{K}{u} P(\sigma, u)$. Here we present one of the equations we used to get the time

dependence of the densities at (90)

$$\frac{d\hat{P}^t(\sigma,u)}{dt} = -r(K,u)\,\hat{P}^t(\sigma,u) + r(K,K-u)\,\hat{P}^t(-\sigma,K-u)(K-u)\,\langle r(K,u')\rangle_{\sigma,\sigma}\,\hat{P}^t(\sigma,u) + (u+1)\,\langle r(K,u')\rangle_{-\sigma,\sigma} \times \hat{P}^t(\sigma,u+1) - u\,\langle r(K,u')\rangle_{-\sigma,\sigma}\,\hat{P}^t(\sigma,u) + (K-u+1)\,\langle r(K,u')\rangle_{\sigma,\sigma}\,\hat{P}^t(\sigma,\hat{u}-1), \tag{92}$$

where we have assumed that $1 \leqslant u \leqslant K-1$ and used the averages $\langle r(K,u')\rangle_{\sigma,\sigma'} = \sum_{u'=0}^{K-1} r(K,u')\,\hat{p}^t(u'|\sigma\,||\,\sigma')$. The equations for $u = 0, K$ are easily obtained from (92) by suppressing its second or third line, respectively.

Equation (92) is analogous to (87) not only because they both give the time derivative of the same quantities but also because they have similar structures. The main difference is that we have made the approximation

$$\hat{P}^t(\sigma,u)\,\hat{P}^t(u'|\sigma',\sigma,u) \approx \hat{P}^t(\sigma,u)\,\hat{p}^t(u'|\sigma',\sigma) \approx \hat{P}^t(\sigma,u)\,\hat{p}^t(u'|\sigma'\,||\,\sigma). \tag{93}$$

The closure (93) works as a substitution drawn from our dynamic cavity method for the conditional probabilities $\hat{P}^t(u'|\sigma',\sigma,u)$. The densities $\hat{p}^t(\hat{u}|\sigma\,||\,\sigma')$ can be obtained from our cavity treatment (see Appendix C). On the other hand, closures (88) and (89) of DINA are the substitutions for $\hat{P}^t(u'|\sigma',\sigma,u)$ that correspond to the assumptions of DRT.

The main panels of Fig. 7 show a comparison between approximations in the first, second, and third levels of our dynamic cavity method and the DINA. Each level is defined by the approximation we use to obtain the cavity probability densities $\hat{p}^t(\hat{u}|\sigma\,||\,\sigma')$. As the level increases, our method predicts a time dependence of the magnetization which is closer to what is obtained from DINA. This means that our cavity closure on the densities $\hat{p}^t(\hat{u}|\sigma\,||\,\sigma')$ becomes similar to the DRT-like closures (88) and (89), which work very well in this case.

C. Susceptible-infectious-susceptible model for epidemics

The propagation of an epidemic is a relevant issue present in various scenarios. Problems like the dissemination of a disease within a population [29] or the spreading of a computer virus or rumors over a network [30] are studied by numerous scientists all over the world. We do not have to explain the significance that the global COVID-19 pandemic has brought nowadays to the development of theoretical tools for understanding epidemic outbreaks [31].

There are a vast variety of models for epidemic processes. Since the seminal work by Kermack and McKendric [32] about the susceptible-infectious-recovered (SIR) model, we are used to seeing compartment models whose main idea is to divide the population into several groups. Each one of those groups is assumed to be homogeneous, in the sense that all individuals interact with rules that depend on which group they belong to. However, this does not necessarily mean that all of members of a compartment are equivalent. The dynamics, for example, can be defined over a specific contact network. Here, we will concentrate on the SIS model defined over random regular graphs.

The standard SIS uses two compartments (states) $x_i = 0 \equiv$ susceptible, or $x_i = 1 \equiv$ infectious and is the simplest model for recurrent transmissible diseases. The epidemic is thus a continuous-time stochastic process with only two admitted transitions. An infectious node transmits the disease to each one of its neighbors with rate β and recovers with rate μ, as represented in Fig. 8. The ratio $\lambda = \beta/\mu$, known as spreading rate, is commonly used as the control parameter of the model.

Such stochastic process can be described by a master equation like (27), where the relevant quantities are probability densities over discrete variables: $P^t(\vec{x})$. This allows us to apply our dynamic cavity method here, and, as said before, we only have to adapt the rates:

$$r_i(x_i, x_{\partial i}) = \beta\,\delta_{x_i,0}\sum_{k\in\partial i} x_k + \mu\,\delta_{x_i,1}. \tag{94}$$

The probability per time unit that x_i changes its value, $r_i(x_i, x_{\partial i})$, is equal to μ when node i is infectious ($x_i = 1$), and is equal to β times the number of infected neighbors of i when the node is occupied by a susceptible individual ($x_i = 0$). This corresponds with our description of the model.

The dynamics of SIS on random networks has motivated abundant literature. One of the most successful theoretical approaches in this scenario is known as quenched mean-field (QMF) theory [33,34], which allows calculating the epidemics threshold by complementing the master equation with some suitable factorization. The most accurate version of QMF is pair quenched mean field (PQMF), or pair-based mean-field. This approximation considers pair correlations and has been intensively investigated lately [35,36] with very good results.

The PQMF equations read

$$\frac{d\rho_i}{dt} = -\mu\rho_i + \beta\sum_{j\in\partial i}(\rho_j - \psi_{ij}) \tag{95}$$

and

$$\frac{d\psi_{ij}}{dt} = -2(\mu+\beta)\psi_{ij} + \beta(\rho_i+\rho_j) + \beta\frac{\rho_j-\psi_{ij}}{1-\rho_i} \times \sum_{k\in\partial i\setminus j}(\rho_k - \psi_{ik}) + \beta\frac{\rho_i-\psi_{ij}}{1-\rho_j}\sum_{k\in\partial j\setminus i}(\rho_k-\psi_{jk}), \tag{96}$$

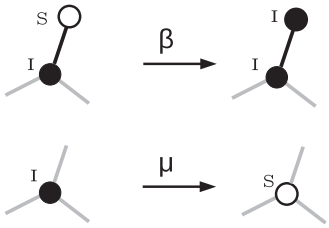

FIG. 8. Allowed transitions in SIS compartment model on networks.

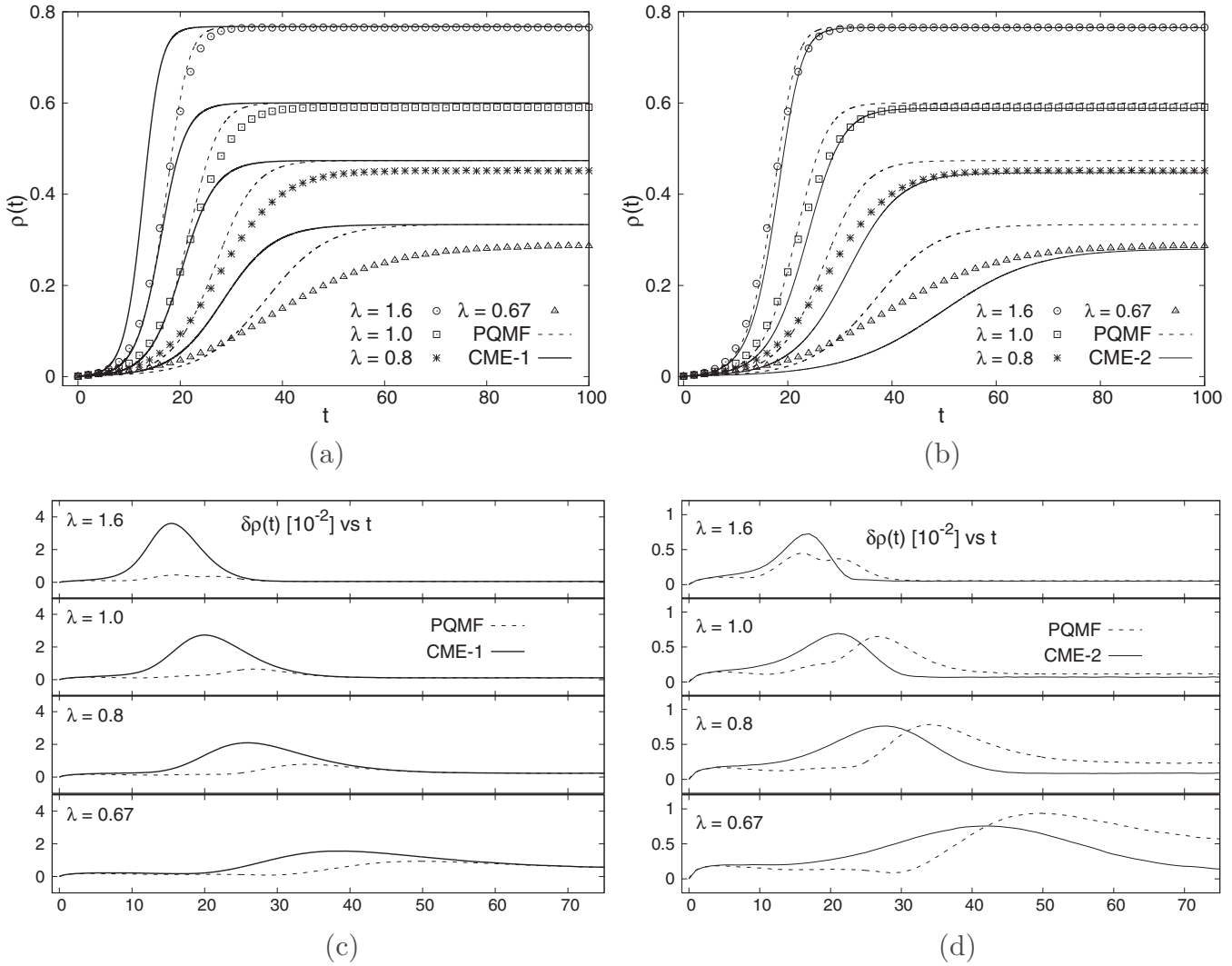

FIG. 9. Dynamics of the SIS model for epidemics according to kinetic Monte Carlo simulations (points), the integration of PQMF (dashed lines), and equations in the first (CME-1, thick lines) and second (CME-2, thin lines) levels of our dynamic cavity method. Calculations were done for $\beta = 0.4$ and $\mu = 0.25, 0.4, 0.5, 0.6$ (that in the figure correspond to $\lambda = 1.6, 1.0, 0.8, 0.67$). In all cases, the infection started in one node of a random regular graph of size $N = 1000$ with connectivity $K = 3$.(a), (b) Time evolution of system's average $\rho(t) = \frac{1}{N}\sum_i \rho_i(t)$. (c), (d) Time evolution of the local error [computed analogously to (84)] between these semianalytical methods and kinetic Monte Carlo simulations.

where $\rho_i(t) = \sum_{x_i} x_i P^t(x_i)$ and $\psi_{ij}(t) = \sum_{x_i}\sum_{x_j} x_i x_j P^t(x_i, x_j)$.

An extensive comparison with equations in the first level of approximation of our dynamic cavity method [see (63) and (64)] has been already carried out in Ref. [37]. As shown there, PQMF gives more accurate predictions for the system's observables. Left panels of Fig. 9 illustrate this for the particular case of an epidemic outbreak that begins with a single infectious individual in a random regular graph of size $N = 1000$ and connectivity $K = 3$. Although the steady state seems to be similarly predicted, PQMF performs indisputably better at the transient regime than the equations in CME-1. The corresponding maximum local errors, depicted in the bottom-left panel, are approximately four times bigger for the latter than for PQMF.

The right panels of Fig. 9 compare kinetic Monte Carlo simulations with PQMF results and the numeric integration of our dynamic cavity equations at the second level of approximation. Equations (66)–(70) give a very good description of the simulated epidemic outbreak. The bottom-right panel shows that its maximum local errors are of the same order as PQMFs, and for $\lambda \leqslant 1.0$ is clear that our cavity method gives even preciser predictions for the steady-state probability densities. This is also observable in the top-right panel of the figure, which illustrates the time dependence of the average of ρ_i over all sites. There we can also see that PQMF does not capture the transient regime appreciably better than our approach.

Thus, the second level of our dynamic cavity method outperforms PQMF at least in describing the propagation of epidemics through a random regular graph. Nevertheless, we expect the same to happen in other families of random networks, like Erdos-Renyi graphs. As PQMF is currently the state-of-the-art among mean-field approximations for the SIS dynamics [35,36], this is a very relevant result.

V. CONCLUSIONS

We derived, using the TRPP, a hierarchical scheme of CMEs directly applicable to the continuous-time dynamics of systems with discrete variables. We carefully described the approximations made at each level of the scheme and explained their significance, pointing to the system's correlation length as the parameter defining the accuracy of the approximation. Our scheme clarifies some of the contents and approximations made in recent literature about CMEs [5–7,13].

We performed numerical tests at different levels of the approximation in spin and epidemic models. For spin models, the accuracy of the technique is comparable with the ones obtained with well-known successful methods like dynamic independent neighbor approximation and DRT, and improves as we increase the level of approximation. Studying the SIS model for epidemics, we show that our equations give better predictions for the stationary state of the epidemics than the widely used PQMF approximation, and, depending on the parameters, can also perform better in the transient regime.

ACKNOWLEDGMENTS

This work was supported by the project Mathematical Modelling of Epidemics, from PNCB CITMA, Republic of Cuba. We thank an anonymous referee for pointing us directly to the derivation in Appendix A.

APPENDIX A: SIMPLE DERIVATION OF THE EQUATION FOR LOCAL PROBABILITY DENSITIES

Equation (53) can be obtained through procedures much simpler than the one used in Sec. III B.

Let S be a subset of the set of nodes of the system $\{1,\dots,N\}$. The notation σ_S stands for the configuration of the variables in S. Assume an arbitrary single spin-flip dynamics, with the rate of flipping of the ith variable depending on σ_i and on $\sigma_{\partial i}$, which defines ∂i, i.e.,

$$\frac{dP^t(\vec{\sigma})}{dt} = \sum_{i=1}^{N}[-r_i(\sigma_i,\sigma_{\partial i})P^t(\vec{\sigma}) + r_i(-\sigma_i,\sigma_{\partial i})P^t(F_i(\vec{\sigma}))]. \tag{A1}$$

Consider now the marginal distribution of the variables in S,

$$P^t(\sigma_S) = \sum_{\sigma_{\bar{S}}} P^t(\sigma_S,\sigma_{\bar{S}}), \tag{A2}$$

with $\bar{S}$ the variables not in S.

When we do this marginalization on the right-hand side of the full master equations, three cases occur:

(1) If $i \notin S$, the two terms compensate by flipping σ_i in the mute index of summation $\sigma_{\bar{S}}$.

(2) If $i \in S$ and $\partial i \subset S$, the marginalization goes through r_i and only acts on P^t, which gives the marginal distribution.

(3) If $i \in S$ and $\partial i \cap \bar{S} \equiv n_i \neq \emptyset$, one only marginalizes over the variables in $\bar{S} \setminus n_i$, where n_i has been defined as the set of neighbors of i which are not in S.

This leads immediately to

$$\frac{dP^t(\sigma_S)}{dt} = \sum_{i\in S:n_i=\emptyset}[-r_i(\sigma_i,\sigma_{\partial i})P^t(\sigma_S) + r_i(-\sigma_i,\sigma_{\partial i})P^t(F_i(\sigma_S))] + \sum_{i\in S:n_i\neq\emptyset}\sum_{\sigma_{n_i}}\left[-r_i(\sigma_i,\sigma_{\partial i})P^t\left(\sigma_S,\sigma_{n_i}\right) + r_i(-\sigma_i,\sigma_{\partial i})P^t\left(F_i(\sigma_S),\sigma_{n_i}\right)\right]. \tag{A3}$$

This is exact for any single spin-flip dynamics, not necessarily on treelike graphs, and for any subset of variables S, and gives back (53) with $S = \mathcal{O}\cup\mathcal{I}$, the variables in $\mathcal{I}$ being those with $n_i = \emptyset$.

APPENDIX B: CONNECTING CAVITY MESSAGES WITH INSTANTANEOUS MAGNITUDES

For completeness, let us reproduce the derivation of Eq. (46) that appears in Ref. [5].

If we marginalize (30) on $X_{\partial i\setminus\{i,j\}}$ and combine the result with (32), we get a cavity message passing equation:

$$\mu^t_{i\to(ij)}(X_i|X_j) = \sum_{\{X_k\},k\in\partial i\setminus j}\Phi^t_i(X_i|X_{\partial i})\prod_{k\in\partial i\setminus j}\mu^t_{k\to(ki)}(X_k|X_i), \tag{B1}$$

where $X_i(t)$ is the history of spin i to time t. To simplify the notation, we will sometimes write $\mu^t_{i\to(ij)}$ for the cavity conditional message.

We have learned that probability densities in the random point processes formulation can be written as [see Eq. (33)]

$$\mu^t_{i\to(ij)}(X_i|X_j) = \prod_{l_i=1}^{s_i}\lambda_{i\to(ij)}\left(X_i,X_j,t_{l_i}\right) - \exp\left\{\int_{t_0}^{t}\lambda_{i\to(ij)}(X_i,X_j,\tau)d\tau\right\}. \tag{B2}$$

Changing indexes accordingly, we can use the same parametrization for the other cavity messages in the update equation.

The interaction term $\Phi^t_i(X_i|X_{\partial i})$ can be interpreted as the probability density of X_i conditioned on the histories of spins in ∂i:

$$\Phi^t_i(X_i|X_{\partial i}) = \prod_{l_i=1}^{s_i} r_i(\sigma_i(t_{l_i}),\sigma_{\partial i}(t_{l_i})) \times \exp\left\{-\int_{t_0}^{t} r_i(\sigma_i(\tau),\sigma_{\partial i}(\tau))d\tau\right\}. \tag{B3}$$

Here, r_i is the real jumping rate of i. Under a Markov assumption this is an instantaneous quantity, meaning that at time τ it depends only on the values of $\sigma_i(\tau)$, $\sigma_{\partial i}(\tau)$.

The trace on the right hand side of (B1) can be written in more detail. Let F be the argument of the sum:

$$\sum_{\{X_k\},k\in\partial i\setminus j}^{[t_0,t]} F(X_i, X_{\partial i}, t)$$
$$= \sum_{\{s_k\},k\in\partial i\setminus j}\left[\prod_{k=1}^{d}\int_{t_0}^{t} dt_1^k \int_{t_1^k}^{t} dt_2^k \ldots \int_{t_{s_k-1}^k}^{t} dt_{s_k}^k\right] F(X_i, X_{\partial i}, t). \tag{B4}$$

In all equations, s_k will be the number of jumps of the history of spin k.

If we write (B1) for every pair (i, j) in the network, we get a system of coupled equations. Having these functions, we could describe all the dynamics of the system. However, (B1) is a very involved expression and we need to transform it to a more tractable one. With that objective, we will differentiate both sides of (B1).

Differentiation in this context should be handled carefully since increasing t means we are changing the sample space itself. Therefore, it is safer to use the definition of differentiation for both sides of Eq. (B1). We will compute the limit:

$$\lim_{\Delta t\to 0}\frac{\mu^{t+\Delta t}_{i\to(ij)}(X_i|X_j) - \mu^{t}_{i\to(ij)}(X_i|X_j)}{\Delta t}. \tag{B5}$$

A very important question arises at this point. What is the relation of $(X_i(t+\Delta t), X_j(t+\Delta t))$ and $(X_i(t), X_j(t))$? Or, in other words, what happens in the interval $(t, t+\Delta t)$? The answer is important because expressions for $\mu^{t+\Delta t}_{i\to(ij)}$ are different whether we consider there can be jumps in the small Δt interval or not. The first thing that makes sense to impose is that histories must agree up to time t. In $(t, t+\Delta t)$ we can have several combinations.

An implicit assumption throughout all this theory is that on an infinitesimal interval only two things can happen to a spin: it can stay on its current state or make one and only one jump to the opposite orientation. Two or more jumps are not allowed. Considering this, we have four cases to analyze:

(1) There are s_i, s_j jumps in (t_0, t) and neither i nor j jumps in $(t, t+\Delta t)$. This occurs with a probability $(1-\lambda_i\Delta t)(1-\lambda_j\Delta t)$.

(2) There are s_i, s_j jumps in (t_0, t) and i XOR j jumps in $(t, t+\Delta t)$. This occurs with a probability $(1-\lambda_i\Delta t)(\lambda_j\Delta t)$ or $(1-\lambda_j\Delta t)(\lambda_i\Delta t)$. These are two cases in one.

(3) There are s_i, s_j jumps in (t_0, t) and both i and j jumps in $(t, t+\Delta t)$. This has a probability of $\lambda_j\lambda_i\Delta t^2$.

When Δt goes to zero, from the previous analysis we conclude that the derivative should be computed, with probability 1, using the first option, where histories for i and j have no jumps in the interval of length Δt.

To differentiate the left hand side of (B1) we can use the parametrization (B2):

$$\mu^{t+\Delta t}_{i\to(ij)} = \prod_{l_i=1}^{s_i}\lambda_{i\to(ij)}(t_{l_i})\exp\left\{-\int_{t_0}^{t+\Delta t}\lambda_{i\to(ij)}(\tau)d\tau\right\},$$
$$\mu^{t+\Delta t}_{i\to(ij)} = [1-\lambda_{i\to(ij)}(t)\Delta t]\prod_{l_i=1}^{s_i}\lambda_{i\to(ij)}(t_{l_i})\exp\left\{-\int_{t_0}^{t}\lambda_{i\to(ij)}(\tau)d\tau\right\} + o(\Delta t),$$
$$\mu^{t+\Delta t}_{i\to(ij)} = [1-\lambda_{i\to(ij)}(t)\Delta t]\,\mu^{t}_{i\to(ij)} + o(\Delta t). \tag{B6}$$

Then, with probability 1, the time derivative of the left-hand side of equation (B1) is equal to $-\lambda_{i\to(ij)}(t)\,\mu^t_{i\to(ij)}$.

To calculate the derivative of the right-hand side of (B1), we should compute

$$\lim_{\Delta t\to 0}\frac{\sum^{[t_0,t+\Delta t]}_{\{X_k\},k\in\partial i\setminus j} F(X_i, X_{\partial i}, t+\Delta t) - \mu^t_{i\to(ij)}}{\Delta t}. \tag{B7}$$

Let us focus on the first term of the numerator in the previous expression. It can be expanded to the first order in Δt. It is important to remember that Δt appears in the integration limits as well as in the integrand F. In addition, we should keep in mind that all jumps for X_i and X_j must occur before t. This restriction, however, does not apply to the histories X_k for k in $\partial i \setminus j$.

The expansion of (B7) can be explained as follows. First, let us remember that F is the joint probability of X_i and $\{X_k\}$ with $k \in \partial i \setminus j$, conditioned on X_j. All histories in the term of interest are in the interval $[t_0, t+\Delta t]$. The expression

$$\sum_{\{X_k\},k\in\partial i\setminus j}^{[t_0,t+\Delta t]} F(X_i, X_{\partial i}, t+\Delta t) \tag{B8}$$

is the marginalization of the mentioned joint probability distribution. The previous sum, to order Δt, has two main contributions. One comes from summing over $\{X_k\}$ with all X_k having no jumps in $[t, t+\Delta t]$:

$$A = \sum_{\{X_k\},k\in\partial i\setminus j}^{[t_0,t]} F(X_i, X_{\partial i}, t)\left\{1-\left[\sum_k \lambda_{k\to(ki)}(t) + r_i(t)\right]\Delta t\right\}. \tag{B9}$$

The other considers all the possibilities of having one of the X_k with a jump in the interval of length Δt:

$$B = \sum_k \sum_{\{X_k\},k\in\partial i\setminus j}^{[t_0,t]} F(X_i, X_{\partial i}, t)\lambda_{k\to(ki)}(t)\Delta t. \tag{B10}$$

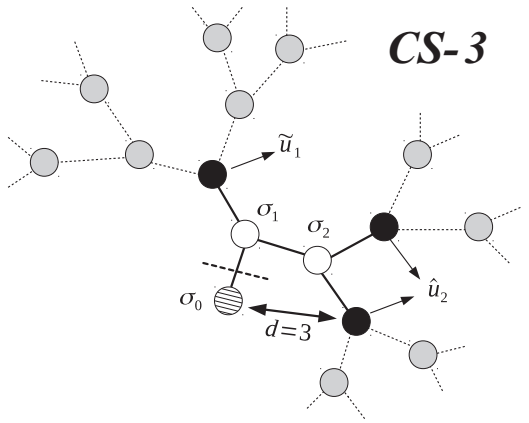

FIG. 10. The cavity probability density $p^t(\hat{u}_2, \sigma_2, \tilde{u}_1, \sigma_1 \,||\, \sigma_0)$ is defined over a connected set in CS-3. This figure illustrates meaning of each one of the variables $\hat{u}_2$, σ_2, $\tilde{u}_1$, σ_1, and σ_0.

Then,

$$\sum_{\{X_k\},k\in\partial i\setminus j}^{[t_0,t+\Delta t]} F(X_i, X_{\partial i}, t+\Delta t) = A + B + o(\Delta t). \tag{B11}$$

Putting all together, we see that B cancels out with the λ part of A, and the remaining term of order 1 is $\mu_{i\to(ij)}(X_i(t)|X_j(t))$, which cancels when inserted in the limit expression.

The final outcome of this differentiation process is

$$\lambda_{i\to(ij)}[X_i, X_j, t]\;\; \mu^t_{i\to(ij)}(X_i|X_j) = \sum_{\{X_k\},k\in\partial i\setminus j}^{[t_0,t]} r_i[\sigma_i(t), \sigma_j(t), \sigma_{\partial i\setminus j}(t)]F(X_i, X_{\partial i}, t). \tag{B12}$$

We can now marginalize the right-hand side of the above equation over all the histories of the spins $k \in \partial i \setminus j$ by keeping the configuration of these spins at the last time t fixed. The result reads

$$\lambda_{i\to(ij)}(X_i, X_j, t)\; \mu^t_{i\to(ij)}(X_i|X_j) = \sum_{\sigma_{\partial i\setminus j}} r_i(\sigma_i(t), \sigma_j(t), \sigma_{\partial i\setminus j})\, p^t(\sigma_{\partial i\setminus j}, X_i \,||\, X_j), \tag{B13}$$

where we introduced the function p as the marginalization of the function F over all the spin histories of the neighbors of i except j, with the configuration at the final time fixed. Note that the notation $\sigma_{\partial i\setminus j}(t)$ is equivalent to $\{\sigma_k(t)\}k \in \partial i \setminus j$ and that in p above appears again explicitly the conditional nature of the probability distribution F.

Equation (B13) represents the differential dynamic message-passing update equation obtained by differentiating (B1) in time. It connects the derivative of the dynamic message $\mu^t_{i\to(ij)}$, and so the jumping rate $\lambda_{i\to(ij)}(t)$ of spin i in the cavity used to parametrize the message in (B2), with the transition rate of the same spin $r_i(\sigma_i(t), \sigma_j(t), \sigma_{\partial i\setminus j}(t))$ at time t.

APPENDIX C: AVERAGE DYNAMIC CAVITY EQUATIONS IN RANDOM REGULAR GRAPHS

Whenever we have initial conditions independent of the site and homogeneous node connectivity, the equations of our dynamic cavity method acquire a spatial symmetry that will allow us to reduce them to a few average case equations. Let us show this through an example.

We will start with Eq. (66):

$$\frac{dp^t(\sigma_{\partial i\setminus j}, \sigma_i \,||\, \sigma_j)}{dt} = -r_i(\sigma_i, \sigma_{\partial i})\, p^t(\sigma_{\partial i\setminus j}, \sigma_i \,||\, \sigma_j) + r_i(-\sigma_i, \sigma_{\partial i})\, p^t(\sigma_{\partial i\setminus j}, -\sigma_i \,||\, \sigma_j) - \sum_{l\in\partial i\setminus j}\sum_{\sigma_{\partial l\setminus i}}\{r_l(\sigma_l, \sigma_{\partial l}) \times p^t(\sigma_{\partial l\setminus i}|\sigma_l \,||\, \sigma_i)\, p^t(\sigma_{\partial i\setminus j}, \sigma_i \,||\, \sigma_j) - r_l(-\sigma_l, \sigma_{\partial l})\, p^t(\sigma_{\partial l\setminus i}|-\sigma_l \,||\, \sigma_i)\, p^t(F_l[\sigma_{\partial i\setminus j}], \sigma_i \,||\, \sigma_j)\}. \tag{C1}$$

In a random regular graph with connectivity K, a spatial symmetry results from choosing an initial condition for $p^t(\sigma_{\partial i\setminus j}, \sigma_i \,||\, \sigma_j)$ which does not depend on i and j. In that case, the equation governing the time evolution of $p^t(\sigma_{\partial i\setminus j}, \sigma_i \,||\, \sigma_j)$ will not depend on the values of i, j for any time. We can write a single equation for all sites:

$$\begin{aligned}\frac{dp^t(\hat{u}, \sigma \,||\, \sigma')}{dt} &= -r(K, \hat{u} + \delta_{\sigma,-\sigma'})\, p^t(\hat{u}, \sigma \,||\, \sigma') + r(K, K - \hat{u} - \delta_{\sigma,-\sigma'})\, p^t(K - \hat{u}, -\sigma \,||\, \sigma') \\ &- (K - 1 - \hat{u})\sum_{u'=0}^{K-1}\binom{K-1}{u'} r(K, u')\{p^t(u'|\sigma \,||\sigma)\, p^t(\hat{u}, \sigma \,||\, \sigma') - p^t(u'|-\sigma \,||\sigma)\, p^t(\hat{u}+1, \sigma \,||\, \sigma')\} \\ &- \hat{u}\sum_{u'=0}^{K-1}\binom{K-1}{u'} r(K, u')\{p^t(u'|-\sigma \,||\sigma)\, p^t(\hat{u}, \sigma \,||\, \sigma') - p^t(u'|\sigma \,||\sigma)\, p^t(\hat{u}-1, \sigma \,||\, \sigma')\}.\end{aligned} \tag{C2}$$

In (C2), regardless of the site where they are defined, the probability densities depend only on two connected spin variables, σ and σ', and on the number $\hat{u} = 0, \ldots, K-1$ of unsatisfied interactions that σ has with its neighbors other than σ'. The sum in the fourth and fifth lines takes into account that $\hat{u}$ unsatisfied interactions, all of which contribute equally to the derivative. The same happens with the second and third lines and the contribution of the remaining $(K - 1 - \hat{u})$ satisfied interactions.

So far, we have not defined new probability densities, we just redenoted $p^t(\sigma_{\partial i\setminus j}, \sigma_i \,||\, \sigma_j)$ into $p^t(\hat{u}, \sigma \,||\, \sigma')$ after realizing that the values of sites i and j where irrelevant due to spatial symmetry, and that it was not important to keep track of all the combinations of $\sigma_{\partial i\setminus j}$, we needed only to record the number of unsatisfied $\hat{u}$ interactions between $\sigma_{\partial i\setminus j}$ and σ_i. Now, we will introduce the total densities $\hat{p}^t(\hat{u}, \sigma \,||\, \sigma') = \binom{K-1}{\hat{u}} p^t(\hat{u}, \sigma \,||\, \sigma')$, noticing that these are analogous to the average probability

densities in (90). Actually, exactly as before, we have

$$\hat{p}^t(\hat{u},\sigma\,||\,\sigma') = \lim_{N\to\infty} \ll \frac{1}{NK}\sum_{i=1}^{N}\sum_{j\in\partial i}\sum_{\sigma_i}\sum_{\sigma_j}\sum_{\sigma_{\partial i\setminus j}} p^t_{\xi_K(N)}(\sigma_{\partial i\setminus j},\sigma_i\,||\,\sigma_j)\,\delta_{\sigma,\sigma_i}\delta_{\sigma',\sigma_j}\;\delta_{(\sum_{k\in\partial i\setminus j}\sigma_k),K-1-2\hat{u}} \gg_{\xi_K(N)}, \tag{C3}$$

where $\xi_K(N)$ is the ensemble of random regular graphs with connectivity K and size N. The symbol $\ll\cdot\gg_{\xi_K(N)}$ represents an average over this ensemble, with proper probabilistic weights.

The differential equation for this average probability densities is

$$\begin{aligned}\frac{d\hat{p}^t(\hat{u},\sigma\,||\,\sigma')}{dt} &= -r(K,\hat{u}+\delta_{\sigma,-\sigma'})\,\hat{p}^t(\hat{u},\sigma\,||\,\sigma') + r(K,K-\hat{u}-\delta_{\sigma,-\sigma'})\,\hat{p}^t(K-\hat{u},-\sigma\,||\,\sigma')\\ &- (K-1-\hat{u})\,\langle\, r(K,u')\,\rangle_{\sigma,\sigma}\,\hat{p}^t(\hat{u},\sigma\,||\,\sigma') + (\hat{u}+1)\,\langle\, r(K,u')\,\rangle_{-\sigma,\sigma}\,\hat{p}^t(\hat{u}+1,\sigma\,||\,\sigma')\\ &- \hat{u}\,\langle\, r(K,u')\,\rangle_{-\sigma,\sigma}\,\hat{p}^t(\hat{u},\sigma\,||\,\sigma') + (K-\hat{u})\,\langle\, r(K,u')\,\rangle_{\sigma,\sigma}\,\hat{p}^t(\hat{u}-1,\sigma\,||\,\sigma'),\end{aligned} \tag{C4}$$

where we have written the averages $\langle\, r(K,u')\,\rangle_{\sigma,\sigma'} = \sum_{u'=0}^{K-1} r(K,u')\,\hat{p}^t(u'|\sigma\,||\,\sigma')$. The conditional cavity probability densities in (C4) are

$$\hat{p}^t(\hat{u}|\sigma\,||\,\sigma') = \frac{\hat{p}^t(\hat{u},\sigma\,||\,\sigma')}{\sum_{u'}\hat{p}^t(u',\sigma\,||\,\sigma')}. \tag{C5}$$

Equations (C4) and (C5) form a closed system that can be numerically integrated. This must be complemented with

$$\begin{aligned}\frac{d\hat{P}^t(\sigma,u)}{dt} &= -r(K,u)\,\hat{P}^t(\sigma,u) + r(K,K-u)\,\hat{P}^t(-\sigma,K-u)\\ &- (K-u)\,\langle\, r(K,u')\,\rangle_{\sigma,\sigma}\,\hat{P}^t(\sigma,u) + (u+1)\,\langle\, r(K,u')\,\rangle_{-\sigma,\sigma}\,\hat{P}^t(\sigma,u+1)\\ &- u\,\langle\, r(K,u')\,\rangle_{-\sigma,\sigma}\,\hat{P}^t(\sigma,u) + (K-u+1)\,\langle\, r(K,u')\,\rangle_{\sigma,\sigma}\,\hat{P}^t(\sigma,\hat{u}-1),\end{aligned} \tag{C6}$$

which can be derived similarly.

To finish writing the equations of the levels of approximation shown Fig. 7 in the main text, we still need to address the first and third levels: CME-1 and CME-3. In the first case, we start with Eqs. (63) and (64)

$$\frac{dp^t(\sigma_i\,||\,\sigma_j)}{dt} = -\sum_{\sigma_{\partial i\setminus j}}\left\{ r_i(\sigma_i,\sigma_{\partial i})\left[\prod_{k\in\partial i\setminus j} p^t(\sigma_k\,||\,\sigma_i)\right] p^t(\sigma_i\,||\,\sigma_j) - r_i(-\sigma_i,\sigma_{\partial i})\left[\prod_{k\in\partial i\setminus j} p^t(\sigma_k\,||\,-\sigma_i)\right] p^t(-\sigma_i\,||\,\sigma_j)\right\}, \tag{C7}$$

$$\frac{dP^t(\sigma_i)}{dt} = -\sum_{\sigma_{\partial i}}\left\{ r_i(\sigma_i,\sigma_{\partial i})\left[\prod_{k\in\partial i} p^t(\sigma_k\,||\sigma_i)\right] P^t(\sigma_i) - r_i(-\sigma_i,\sigma_{\partial i})\left[\prod_{k\in\partial i} p^t(\sigma_k\,||\,-\sigma_i)\right] P^t(-\sigma_i)\right\}. \tag{C8}$$

It is easy to see that the average case versions of this equations at random regular graphs with homogeneous initial conditions are

$$\begin{aligned}\frac{d\hat{p}^t(\sigma\,||\,\sigma')}{dt} &= -\sum_{u'=0}^{K-1}\{r(K,u'+\delta_{\sigma,-\sigma'})[\hat{p}(-\sigma|\sigma)]^{u'}\,[\hat{p}(\sigma|\sigma)]^{K-1-u'}\,\hat{p}^t(\sigma\,||\,\sigma') - r(K,u'+\delta_{\sigma,\sigma'})\\ &\times[\hat{p}(\sigma|-\sigma)]^{u'}\,[\hat{p}(-\sigma|-\sigma)]^{K-1-u'}\,\hat{p}^t(-\sigma\,||\,\sigma')\},\end{aligned} \tag{C9}$$

$$\frac{d\hat{P}^t(\sigma)}{dt} = -\sum_{u'=0}^{K}\left\{r(K,u')\,[\hat{p}(-\sigma|\sigma)]^{u'}\,[\hat{p}(\sigma|\sigma)]^{K-u'}\,\hat{P}^t(\sigma) - r(K,u')\,[\hat{p}(\sigma|-\sigma)]^{u'}\,[\hat{p}(-\sigma|-\sigma)]^{K-u'}\,\hat{P}^t(-\sigma)\right\}. \tag{C10}$$

Equations (C9) and (C10) also form a closed system and its numerical integration is shown in Fig. 7 of the main text. The equations in the third level of approximation, CME-3, whose results appear also in that figure, require some extra work.

Our probability densities are now $p^t(\hat{u}_2,\sigma_2,\tilde{u}_1,\sigma_1\,||\,\sigma_0)$, which are defined over the connected sets illustrated in the bottom-left panel of Fig. 4. The spins σ_0, σ_1, and σ_2 are marked in Fig. 10. The integer $\hat{u}_2$, which goes from zero to $K-1$, represents the number of unsatisfied interactions between σ_2 and its neighbors, without counting σ_1. Finally, the integer $\tilde{u}_1$, which goes from zero to $K-2$, is the number of unsatisfied interactions between σ_1 and its neighbors, without counting σ_0 and σ_2.

As we learned with (58), the exact equations for this densities are

$$\begin{aligned}\frac{dp^t(\hat{u}_2,\sigma_2,\tilde{u}_1,\sigma_1\,||\,\sigma_0)}{dt} &= -r(K,\tilde{u}_1+\delta_{\sigma_0,-\sigma_1}+\delta_{\sigma_2,-\sigma_1})\,p^t(\hat{u}_2,\sigma_2,\tilde{u}_1,\sigma_1\,||\,\sigma_0)\\ &+ r(K,K-\tilde{u}_1-\delta_{\sigma_0,-\sigma_1}-\delta_{\sigma_2,-\sigma_1})\,p^t(\hat{u}_2,\sigma_2,K-2-\tilde{u}_1,-\sigma_1\,||\,\sigma_0)\\ &- r(K,\hat{u}_2+\delta_{\sigma_1,-\sigma_2})\,p^t(\hat{u}_2,\sigma_2,\tilde{u}_1,\sigma_1\,||\,\sigma_0) + r(K,K-\hat{u}_2-\delta_{\sigma_1,-\sigma_2})\,p^t(K-1-\hat{u}_2,-\sigma_2,\tilde{u}_1,\sigma_1\,||\,\sigma_0)\end{aligned}$$

$$
\begin{aligned}
&- (K-2-\tilde{u}_1)\sum_{u_1'=0}^{K-1}\binom{K-1}{u_1'} r(K,u_1')\,\{p^t(u_1'|\hat{u}_2,\sigma_2,\tilde{u}_1,\sigma_1\,||\sigma_0)\,p^t(\hat{u}_2,\sigma_2,\tilde{u}_1,\sigma_1\,||\,\sigma_0)\\
&- p^t(u_1'|\hat{u}_2,\sigma_2,\tilde{u}_1+1,\sigma_1\,||\sigma_0)\,p^t(\hat{u}_2,\sigma_2,\tilde{u}_1+1,\sigma_1\,||\,\sigma_0)\}\\
&- \tilde{u}_1\sum_{u_1'=0}^{K-1}\binom{K-1}{u_1'} r(K,u_1')\,\{p^t(u_1'|\hat{u}_2,\sigma_2,\tilde{u}_1,\sigma_1\,||\sigma_0)\,p^t(\hat{u}_2,\sigma_2,\tilde{u}_1,\sigma_1\,||\,\sigma_0)\\
&- p^t(u_1'|\hat{u}_2,\sigma_2,\tilde{u}_1-1,\sigma_1\,||\sigma_0)\,p^t(\hat{u}_2,\sigma_2,\tilde{u}_1-1,\sigma_1\,||\,\sigma_0)\}\\
&- (K-1-\hat{u}_2)\sum_{u_2'=0}^{K-1}\binom{K-1}{u_2'} r(K,u_2')\,\{p^t(u_2'|\hat{u}_2,\sigma_2,\tilde{u}_1,\sigma_1\,||\sigma_0)\,p^t(\hat{u}_2,\sigma_2,\tilde{u}_1,\sigma_1\,||\,\sigma_0)\\
&- p^t(u_2'|\hat{u}_2+1,\sigma_2,\tilde{u}_1,\sigma_1\,||\sigma_0)\,p^t(\hat{u}_2+1,\sigma_2,\tilde{u}_1,\sigma_1\,||\,\sigma_0)\}\\
&- \hat{u}_2\sum_{u_2'=0}^{K-1}\binom{K-1}{u_2'} r(K,u_2')\,\{p^t(u_2'|\hat{u}_2,\sigma_2,\tilde{u}_1,\sigma_1\,||\sigma_0)\,p^t(\hat{u}_2,\sigma_2,\tilde{u}_1,\sigma_1\,||\,\sigma_0)\\
&- p^t(u_2'|\hat{u}_2-1,\sigma_2,\tilde{u}_1,\sigma_1\,||\sigma_0)\,p^t(\hat{u}_2-1,\sigma_2,\tilde{u}_1,\sigma_1\,||\,\sigma_0)\}. \qquad \text{(C11)}
\end{aligned}
$$

Unlike what we have seen before, our variables are not defined over regular connected sets *rCS-3* (see Fig. 10). We need a slightly different closure, or more specifically, two new closures. These are necessary because the time derivative of densities in *CS-3* that appears in (C11) involves probability densities defined over connected sets in *CS-4*.

The first approximation targets the conditional cavity probability densities that appear in lines 5–8 of (C11) and reduces them to densities of the form $p^t(\hat{u}_2,\sigma_2,\tilde{u}_1,\sigma_1\,||\,\sigma_0)$:

$$
p^t_{\mathrm{SAT}}(u_1'|\hat{u}_2,\sigma_2,\tilde{u}_1,\sigma_1\,||\sigma_0) \approx \frac{p^t(u_1',\sigma_1,\bar{u}_1,\sigma_1\,||\sigma_0)}{\sum_{u'}p^t(u',\sigma_1,\bar{u}_1,\sigma_1\,||\sigma_0)}, \qquad \text{(C12)}
$$

$$
p^t_{\mathrm{UNSAT}}(u_1'|\hat{u}_2,\sigma_2,\tilde{u}_1,\sigma_1\,||\sigma_0) \approx \frac{p^t(u_1',-\sigma_1,\bar{u}_1,\sigma_1\,||\sigma_0)}{\sum_{u'}p^t(u',-\sigma_1,\bar{u}_1,\sigma_1\,||\sigma_0)}. \qquad \text{(C13)}
$$

The left panel of Fig. 11 illustrates Eqs. (C12) and (C13). There, the integer $u_1' = 0,\ldots,K-1$ represents the number of unsatisfied interactions related to a specific neighbor of σ_1 which can either have the same value of σ_1 [Eq. (C12)] or the opposite value $-\sigma_1$ [Eq. (C13)]. On the other hand, $\bar{u}_1 = 0,\ldots,K-2$ is the number of unsatisfied interactions between σ_1 and its neighbors other than σ_0 and the one mentioned in the previous sentence (this means that $\tilde{u}_1$ includes the interaction with σ_2). Notice that we have dropped the dependency on the number of unsatisfied relations $\hat{u}_2$ because the spins involved in that interactions (except σ_2) are at a distance $d = 4 > 3$ from the ones involved in u_1'.

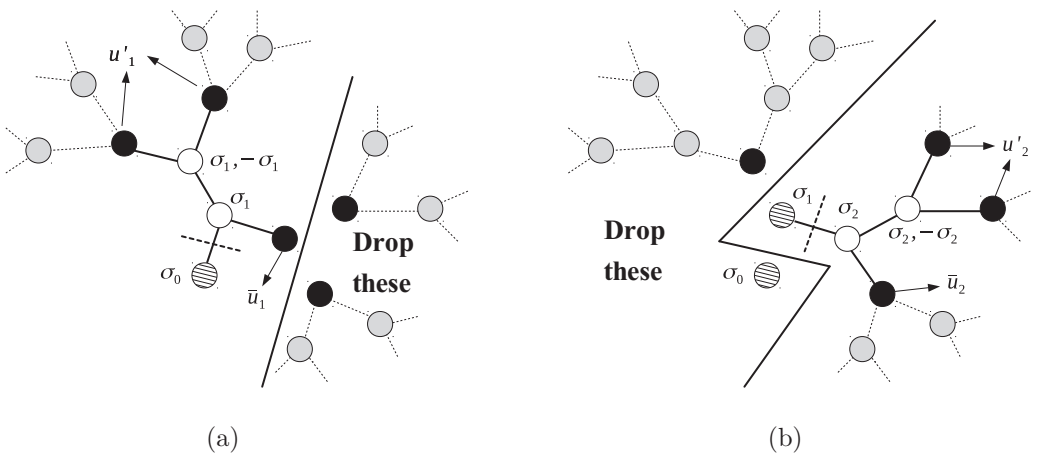

FIG. 11. Illustration of the approximations (C12)–(C15) applied to conditional cavity probability densities. These are necessary because the time derivative (C11) involves probability densities defined over connected sets in *CS-4*. In each panel, the nodes not colored in gray belong to such connected sets, and we have to drop the dependency on some of them to give closure to (C11).

The second approximation targets the conditional cavity probability densities that appear in lines from 9–12 of (C11):

$$p^t_{\rm SAT}(u'_2|\hat{u}_2,\sigma_2,\tilde{u}_1,\sigma_1\,||\sigma_0) \approx \frac{p^t(u'_2,\sigma_2,\bar{u}_2,\sigma_2\,||\sigma_1)}{\sum_{u'} p^t(u',\sigma_2,\bar{u}_2,\sigma_2\,||\sigma_1)}, \tag{C14}$$

$$p^t_{\rm UNSAT}(u'_1|\hat{u}_2,\sigma_2,\tilde{u}_1,\sigma_1\,||\sigma_0) \approx \frac{p^t(u'_2,-\sigma_2,\bar{u}_2,\sigma_2\,||\sigma_1)}{\sum_{u'} p^t(u',-\sigma_2,\bar{u}_2,\sigma_2\,||\sigma_1)}. \tag{C15}$$

The right panel of Fig. 11 illustrates the meaning of this equations. We will not give more details because they are very similar to what we said about (C14) and (C15).

From this point, it is easy to derive equations for the averages $\hat{p}^t(\hat{u}_2,\sigma_2,\tilde{u}_1,\sigma_1\,||\,\sigma_0)$, which together with the averages of closure relations (C12)–(C15) form a system that we can numerically integrate to obtain the results in Fig. 7.

[1] N. G. van Kampen, *Stochastic Processes in Physics and Chemistry* (Elsevier, Amsterdam, 1992), Vol. 1.

[2] D. J. Daley and D. Vere-Jones, *An Introduction to the Theory of Point Processes Volume I: Elementary Theory and Methods* (Springer Science & Business Media, Berlin, 2002).

[3] B. Karrer and M. E. J. Newman, Message Passing Approach for general epidemic models, Phys. Rev. E **82**, 016101 (2010).

[4] M. Shrestha, S. V. Scarpino, and C. Moore, Message-passing approach for recurrent-state epidemic models on networks, Phys. Rev. E **92**, 022821 (2015).

[5] E. Aurell, G. Del Ferraro, E. Domínguez, and R. Mulet, A cavity master equation for the continuous time dynamics of discrete spins models, Phys. Rev. E **95**, 052119 (2017).

[6] E. Aurell, E. Domínguez, D. Machado, and R. Mulet, Exploring the diluted ferromagnetic p-spin model with a cavity master equation, Phys. Rev. E **97**, 050103(R) (2018).

[7] E. Aurell, E. Domínguez, D. Machado, and R. Mulet, A Theory of Non-Equilibrium Local Search on Random Satisfaction Problems, Phys. Rev. Lett. **123**, 230602 (2019).

[8] R. J. Glauber, Time-dependent statistics of the Ising model, J. Math. Phys. **4**, 294 (1963).

[9] A. C. C. Coolen, R. Kühn, and P. Sollich, *Theory of Neural Information Processing Systems* (Oxford University Press, New York, 2005).

[10] A. Crisanti and H. Sompolinsky, Dynamics of spin systems with randomly asymmetric bonds: Ising spins and Glanber dynamics, Phys. Rev. A **37**, 4865 (1988).

[11] H. Rieger, M. Schreckenberg, and J. Zittartz, Glauber dynamics of the asymmetric SK-model, Z. Phys. B: Condens. Matter **74**, 527 (1989).

[12] B. Derrida, E. Gardner, and A. Zippelius, An exactly solvable asymmetric neural network model, Europhys. Lett. **4**, 167 (1987).

[13] E. Domínguez, D. Machado, and R. Mulet, The cavity master equation: Average and fixed point of the ferromagnetic model in random graphs, J. Stat. Mech. (2020) 073304.

[14] A. C. C. Coolen, S. N. Laughton, and D. Sherrington, Dynamical replica theory for disordered spin systems, Phys. Rev. B **53**, 8184 (1996).

[15] S. N. Laughton, A. C. C. Coolen, and D. Sherrington, Order-parameter flow in the SK spin-glass: II. Inclusion of microscopic memory effects, J. Phys. A: Math. Gen. **29**, 763 (1996).

[16] A. Mozeika and A. C. C. Coolen, Dynamical replica analysis of processes on finitely connected random graphs: I. Vertex covering, J. Phys. A: Math. Theor. **41**, 115003 (2008).

[17] A. Mozeika and A. C. C. Coolen, Dynamical replica analysis of processes on finitely connected random graphs: II. Dynamics in the griffiths phase of the diluted Ising ferromagnet, J. Phys. A: Math. Theor. **42**, 195006 (2009).

[18] H. Nishimori and M. Yamana, Dynamical probability distribution function of the SK model at high temperatures, J. Phys. Soc. Jpn. **65**, 3 (1996).

[19] A. C. C. Coolen, S. N. Laughton, and D. Sherrington, Perturbative large deviation analysis of non-equilibrium dynamics, J. Phys. Soc. Jpn. **93**, 084001 (2014).

[20] W. Barthel, A. K. Hartmann, and M. Weigt, Solving satisfiability problems by fluctuations: The dynamics of stochastic local search algorithms, Phys. Rev. E **67**, 066104 (2003).

[21] G. Semerjian and R. Monasson, Relaxation and metastability in a local search procedure for the random satisfiability problem, Phys. Rev. E **67**, 066103 (2003).

[22] G. Semerjian and M. Weigt, Approximation schemes for the dynamics of diluted spin models: The Ising ferromagnet on a Bethe lattice, J. Phys. A: Math. Gen. **37**, 5525 (2004).

[23] C. Kipnis and C. Landim, *Scaling Limits of Interacting Particle Systems* (Springer Verlag, Berlin, Heidelberg, 1999), Vol. 320.

[24] P. Erdős and A. Rényi, On random graphs, Publicationes Mathematicae Debrecen **6**, 290 (1959).

[25] E. Cator and P. Van Mieghem, Second-order mean-field susceptible-infected-susceptible epidemic threshold, Phys. Rev. E **85**, 056111 (2012).

[26] A. S. Mata and S. C. Ferreira, Pair quenched mean-field theory for the susceptible-infected-susceptible model on complex networks, Europhys. Lett. **103**, 48003 (2013).

[27] A. Dembo and A. Montanari, Ising models on locally tree-like graphs, Ann. Appl. Probab. **20**, 565 (2010).

[28] L. Viana and A. J. Bray, Phase diagrams for dilute spin glasses, J. Phys. C **18**, 3037 (1985).

[29] R. Pastor-Satorras, C. Castellano, P. Van Mieghem, and A. Vespignani, Epidemic processes in complex networks, Rev. Mod. Phys. **87**, 925 (2015).

[30] R. Pastor-Satorras and A. Vespignani, Epidemic Spreading in Scale-Free Networks, Phys. Rev. Lett. **86**, 3200 (2001).

[31] E. Cuevas, An agent-based model to evaluate the COVID-19 transmission risks in facilities, Comput. Biol. Med. **121**, 103827 (2020).

[32] W. O. Kermack and A. G. McKendrick, A contribution to the mathematical theory of epidemics, Proc. R. Soc. London, Ser. A **115**, 700 (1927).

[33] P. Van Mieghem, J. Omic, and R. Kooij, Virus spread in networks, IEEE/ACM Trans. Networking **17**, 1 (2009).

[34] C. Castellano and R. Pastor-Satorras, Thresholds for Epidemic Spreading in Networks, Phys. Rev. Lett. **105**, 218701 (2010).

[35] D. H. Silva, S. C. Ferreira, W. Cota, R. Pastor-Satorras, and C. Castellano, Spectral properties and the accuracy of mean-field approaches for epidemics on correlated power-law networks, Phys. Rev. Research **1**, 033024 (2019).

[36] D. H. Silva, F. A. Rodrigues, and S. C. Ferreira, High prevalence regimes in the pair-quenched mean-field theory for the susceptible-infected-susceptible model on networks, Phys. Rev. E **102**, 012313 (2020).

[37] E. Ortega, D. Machado, and A. Lage-Castellanos, Dynamics of epidemic models from cavity master equations, arXiv:2006.15881v2.